

Repeat pass interferometry with PHARUS

J.S. Groot

D. van Halsema

P.J.L Blommaart

G.J. Husti

G.A.M. Kruse

D. van Loon

J. Samson

E.J.O. Schrama

A.J. Striegel

J.M.P.C.M. Visser



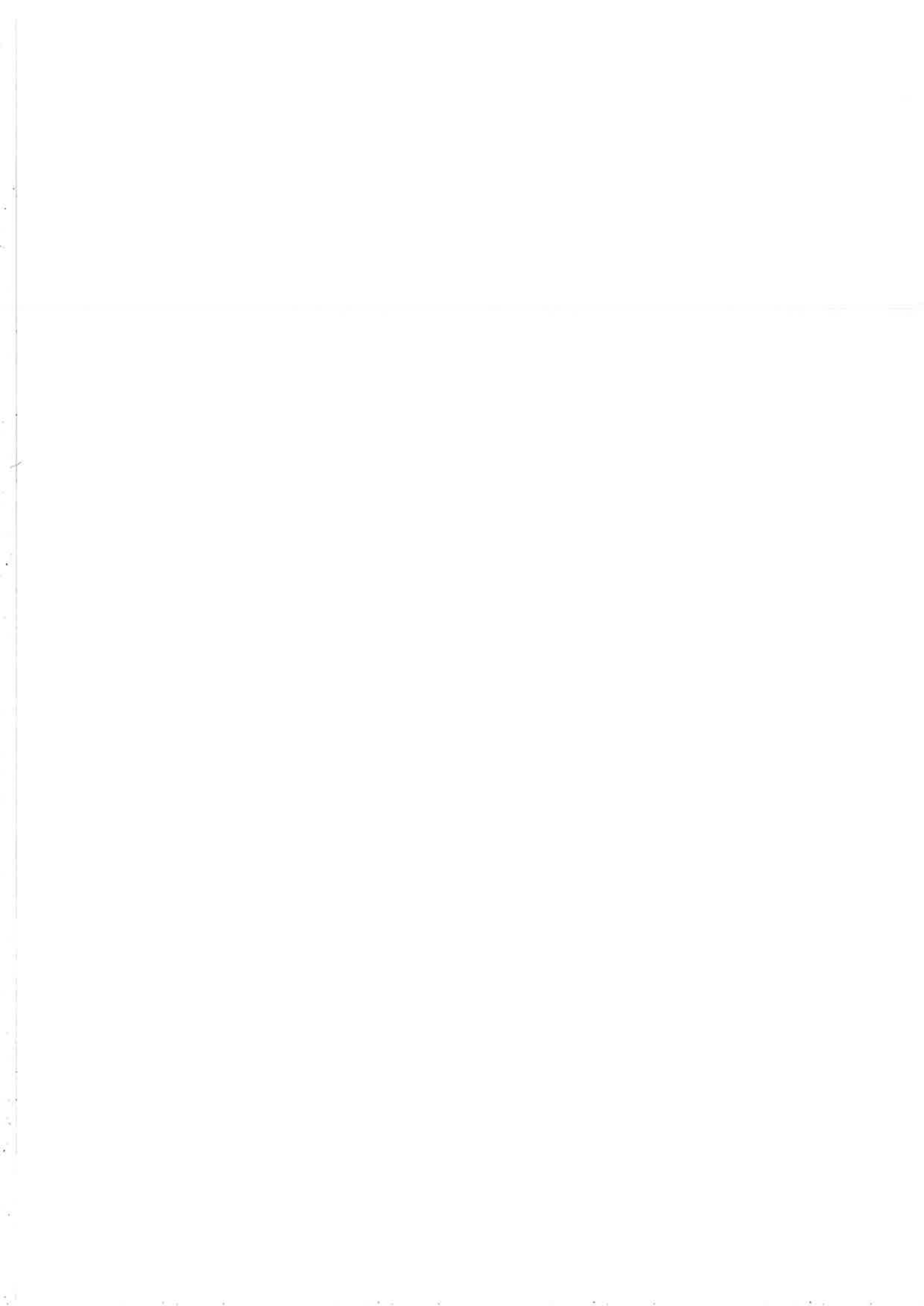
Repeat pass interferometry with PHARUS

J.S. Groot D. van Halsema TNO-FEL P.J.L. Blommaart **RWS** G. J. Husti **TUD DEOS** G.A.M. Kruse GeoDelft D. van Loon **TUD DEOS** J. Samson NLR E.J.O. Schrama **TUD DEOS** A.J. Striegel J.M.P.C.M. Visser NLR

NRSP-2 report 00-23 NRSP-2 project 5.1/TE-54 ISBN 90 54 11 325 1

December 2000

This report describes a project carried out in the framework of the National Remote Sensing Programme (NRSP-2) under responsibility of the Netherlands Remote Sensing Board (BCRS)



Abstract

Title

Repeat pass interferometry with PHARUS

BCRS project

: 5.1/TE54

Date

: October 2000

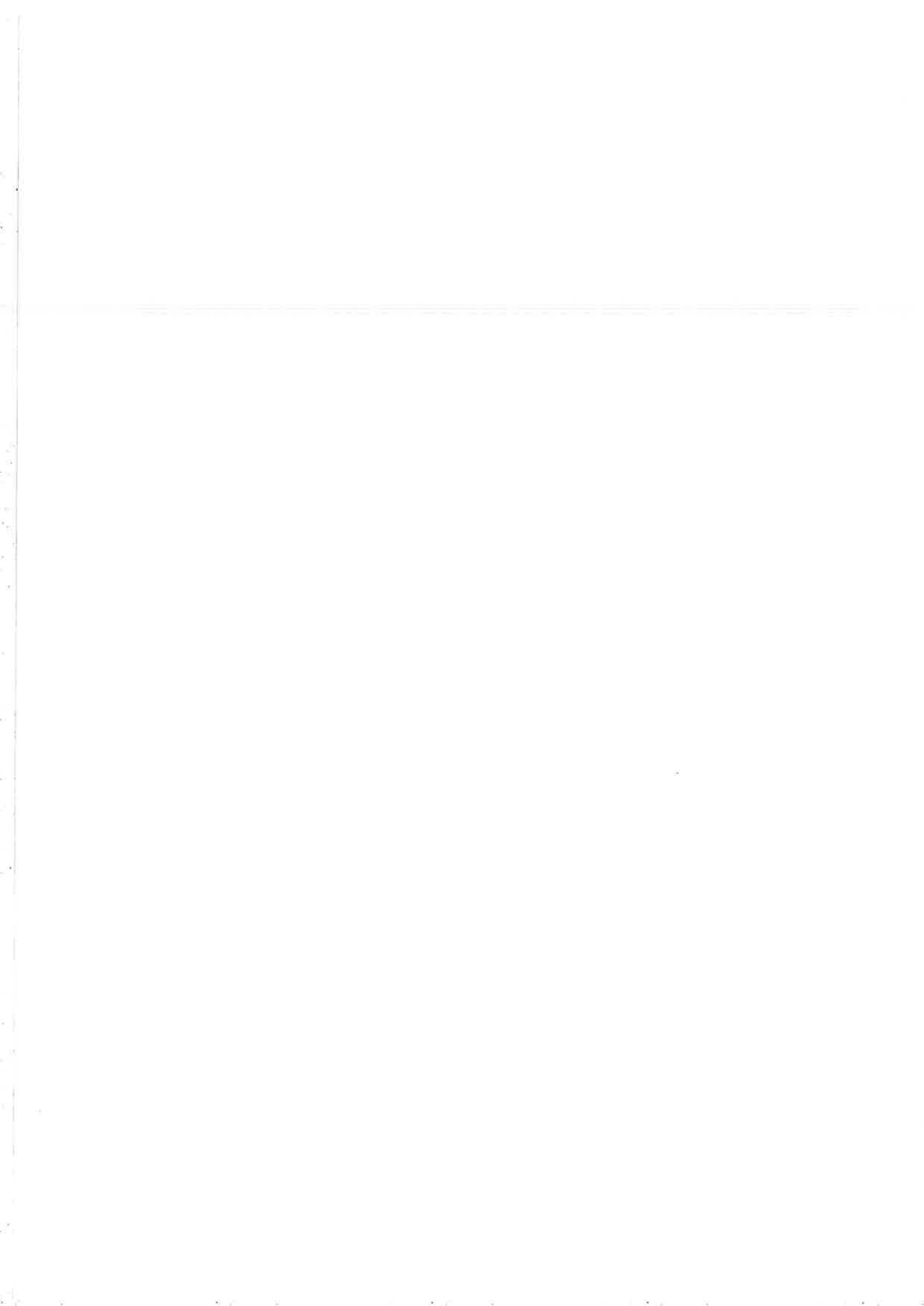
Deformation measurements are important in the field of ground engineering. Deformation can have a nonnatural cause (e.g., surface deformation due to tunnel construction) or a natural one (e.g., dike deformation due to a high water level). Those deformations are usually determined with conventional levelling methods, which are point measurements. Another technique, radar interferometry, can in principle provide deformations with millimetre to centimetre accuracy over large areas (typically $10 \text{ km} \times 10 \text{ km}$). Because of the high water periods of 1993 and 1995, nowadays more attention is paid to accurate dike strength determination methods and the measurement of dike deformation. The response to a questionnaire distributed amongst four representatives of several water boards and one adviser for road maintenance and management indicated that interferometry can be very useful for water defence and road management.

Radar interferometry is the subject of this report. To evaluate its utility an experiment with the PHARUS SAR (Synthetic Aperture Radar) system was set up to measure the deformation of a rapidly deforming (~1 cm per month) dike. These small deformations should be detectable with PHARUS. Several passes with PHARUS were made over the dike on different dates, hence the term "repeat pass interferometry". For successful deformation measurements the tracks and beam directions should be nearly identical. This demands much of the real time track and beam direction control. The demands were planned to be met by using DGPS and electronic beam steering, respectively. In addition, the tracks used for the subsequent SAR processing have to be very accurate. These tracks were computed by combining DGPS and INS measurements.

Three flights were performed, but due to technical shortcomings and bad weather conditions good quality SAR data was available from only one day, 29 January 1999. It turned out that the tracks were accurate enough, although an unwanted oscillation around the reference track was present. The radar beam direction control did not function correctly. Interferograms computed from the data show differences in coherence between water and land, but the phase information (necessary for deformation extraction) was of no use because the phase coherence over land was by far too low caused by erroneous beam steering and processing errors.

For this reason, an extra experiment was carried out on February 3, 2000. This time the beam steering performed much better, though still not optimal. Coherence and phase of the interferogram both contained good, interpretable information. From an interferogram the height of a dike could be estimated with a few decimetres accuracy. Although the interferogram was not yet free from artefacts this proofs that repeat pass interferometry with PHARUS is feasible.

In a next step the deformation measurement capability will be demonstrated, but for that one needs another flight separated in time from the February 3 flight. This flight has been performed in May 2000 and the results will be reported separately in the near future.



Executive summary

Title Repeat pass interferometry with PHARUS

BCRS project 5.1/TE-54

Authors J.S. Groot, D. van Halsema (TNO-FEL), J. Samson, A.J. Striegel, J.M.P.C.M. Visser

(NLR), P.J.L. Blommaart (RWS), G.A.M. Kruse (GeoDelft), G.J. Husti, D. van Loon,

E.J.O. Schrama (TUD DEOS)

Date : October 2000

Deformation measurements are important in the field of ground engineering. Deformation can have a non-natural cause (e.g., surface deformation due to tunnel construction) or a natural one (e.g., dike deformation due to a high water level). Those deformations are usually measured with conventional levelling methods ("waterpassingen"). In this case a single measurement gives a deformation at only one point. Another technique, radar interferometry, can in principle provide deformations with millimetre to centimetre accuracy over large areas. PHARUS, an airborne radar instrument, was used to investigate this technique. PHARUS should be able to provide deformations over about $10 \text{ km} \times 10 \text{ km}$ areas, with a value for every $\sim 1 \times 4 \text{ m}$ patch.

Because of the high water periods of 1993 and 1995, nowadays more attention is paid to accurate dike strength determination methods and the measurement of dike deformation. The response to a questionnaire distributed amongst four representatives of several water boards and one adviser for road maintenance and management indicated that interferometry can be very useful for water defence and road management.

To evaluate the utility of radar interferometry an experiment was set up with PHARUS to measure the deformation of a rapidly deforming (~1 cm per month) dike. These small deformations should be detectable. Several passes (flights) with PHARUS were made over the dike on different dates, hence the term "repeat pass interferometry". For successful deformation measurements the antenna directions and tracks (of two measurements) should be very nearly identical. An everyday life visual counterpart is that e.g. a car simply looks different when viewed from a different angle and/or position. The interferometric mm-cm deformation accuracy can only be attained when the (measurement) difference is exclusively due to the deformation. This limits the antenna direction and track differences.

Measures were taken to limit the antenna direction variations and track differences. The antenna direction was corrected electronically. For example, if the aircraft rotated to the right, the antenna direction was electronically "rotated" to the left with exactly the same amount. The antenna direction is in this way fixed to the geographical north. Track fixation was done by using a differential GPS (meter accuracy) during the flight.

Three flights were performed, but due to technical shortcomings and bad weather conditions good quality SAR data was available from only one day, 29 January 1999. It turned out that the tracks were accurate enough, although an unwanted oscillation was present. The antenna direction control did not function correctly yet.

The data was analysed as usually by the computation of an interferogram. An interferogram was produced from two images separated in time. Ideally, for our purpose the only effect present in an interferogram would be the deformation. However, all kinds of unwanted scene and radar differences also show up. They

hamper easy interpretation and should be minimised. The interferogram showed difference between land and water (because the water surface changes much more rapidly than that of land), which is a kind of minimum demand. However, the data was far from being adequate for deformation extraction. The main causes were erroneous beam steering and processing errors.

For this reason, an extra experiment was carried out on 3 February 2000. This time the beam steering performed much better, though still not optimal. The interferogram contained good, interpretable information. The height of a (6.6 m high) dike could be estimated with a few decimetres accuracy. Although the interferogram was not yet free from disturbances this proofs that repeat pass interferometry with PHARUS is feasible. In a next step the deformation measurement capability will be demonstrated, but for that one needs another flight separated in time from the February 3 flight. This flight has been performed in May 2000 and the results will be reported separately in the near future.

Contents

Exe	cutive si	ımmary		
List	of figur	es	5	
Abł	reviatio	ns	7	
1.	Introduction			
	1.1	Motivation for the experiment	8	
	1.2	SAR interferometry	9	
	1.3	Interferometric deformation measurements	10	
	1.4	Contents of the report		
2.	User requirements			
	2.1	Problems and objective		
	2.2	Activities		
	2.3	Type of dikes, loads and subsoil		
	2.4	Potential failure mechanisms	16	
	2.5	Questionnaire	20	
	2.6	Comparison of airborne InSar measurement with conventional techniques		
3.	Experimental considerations			
	3.1	Orbit and beam direction conditions		
	3.2	Orbit and beam direction control		
	3.3	GPS processing for high accuracy off line orbits	25	
4.	The experiment		31	
	4.1	Location	_	
	4.2	Corner reflectors		
	4.3	Flight lines		
	4.4	Radar mode		
	4.5	Flights performed		
5.	Basic data analysis			
	5.1	GPS orbit data from phase measurements		
	5.2	Horizontal distance between planned and flown tracks		
	5.3	Line of sight (LOS) and depression angle analysis		
	5.4	SAR data		
6.	Interferometric data analysis I			
	6.1	Interferograms		
	6.2	Spectral analysis		
	6.3	Additional findings		

7.	Interferometric data analysis II		52
	7.1	GSP changes	52
	7.2	Results	53
8.	Conclusions and recommendations		55
	8.1	User requirements	55
	8.2	Continuous kinematic GPS by postprocessing using phase measurements	
	8.3	Data analysis	
9.	Refer	ences	59
App	endix A	- Questionnaire (in Dutch)	1
App	endix B	- Responses to questionnaire (in Dutch)	5
App	endix C	- Beam steering	7

List of figures

Figure 1.1:	The PHARUS SAR system used for this experiment. The radar pod is visible below the cockpit.	8
Figure 1.2:	Schematic representation of the repeat pass deformation measurement	
	principle	
Figure 2.1:	Potential failure mechanisms	
Figure 3.1:	Block diagram of navigation hardware	. 24
Figure 3.2:	The equipment in the aircraft (the Trimble 4000 SSi receiver is at the upper-left side)	. 26
Figure 3.3:	Set up of the ground stations in the neighbourhood of Herwijnen	. 26
Figure 3.4:	Flowchart of the PHARUS trajectory software. The 'final trajectory' is the sum of the 4 th order polynomial and the IRS trajectory	.29
Figure 4.1:	Topographic map (with Gorinchem at the right and the dike at the left) and photograph of the dike and its surroundings	
Figure 4.2:	Geotechnical profile of the subsurface in the immediate vicinity of the dike, showing the thick clay and peat deposits whose low strength and high compressibility cause the observed strong deformation. Explanation: Inverted triangles and circles = CPT and borehole; 12 = clay; 4 = peat; 15 = organic clay (flood basin deposits); 9 = basal peat (transgressive); 32 = Sand	
Figure 4.3:	(Pleistocene)	.32
Figure 5.1:	The flight track of the aircraft at 6 km altitude (flight on 29 January 1999)	
Figure 5.2:	Horizontal distances from 33 degree (top) and 63 degree (bottom) planned tracks to the tracks flown. The plots cover the 8 km planned. The horizontal distance is plotted as a function of RDx/10 ⁵ m, not the distance along the track	
Figure 5.3:	Line of sight and depression angles of run 5, plotted as a function of time	
Figure 5.4:	Difference in LOS angle of all possible pairs of runs.	
Figure 5.5:	Image of run 10 (near range at the bottom; dimensions: 6338 m azimuth×5778 m slant range). The lower right part corresponds to the topographic map of Figure 4.1	
Figure 5.6:	Corner reflectors.	.45
Figure 6.1:	Top: amplitude image (the more or less vertical bands are scanner/printer artefacts). Middle: absolute value of the coherence. Bottom: phase of the coherence.	.47
Figure 6.2:	Top: amplitude image. Middle: absolute value of the coherence. Bottom: phase of the coherence.	
Figure 6.3:	Top: amplitude image. Middle: absolute value of the coherence. Bottom:	
Figure 6.4:	Expected coherence loss (top) and actual coherence (bottom) as a function of azimuth position x.	.50
Figure 6.5:	Fragmented corner reflector responses.	51

Figure 7.1:	Magnitude, coherence and unwrapped phase of a small area below De	
	Merwede.	54
Figure C.1:	LOS, track (TRK) and heading (HDG) plotted as a function of time (the unit	
	of the horizontal axis is proportional to time). Note the different scales of	
	the left (LOS) and right (TRK and HDG) axes.	9

Abbreviations

BCRS Netherlands Remote Sensing Board
DGPS Differential Global Positioning System

DWW Road and Hydraulic Engineering Division ('Dienst Weg- en Waterbouwkunde')

ESA European Space Agency

GD GeoDelft (formerly 'Grondmechanica Delft')

HRS Water Board ('Hoogheemraadschap') of the Alblasserwaard and the

Vijfheerenlanden

GPS Global Positioning System
INSAR INterferometric SAR
IRS Inertial Reference System
NLR National Aerospace Laboratory
NRSP National Remote Sensing Programme

OTF On The Fly

PHARUS Polarimetric PHased Array Universal SAR

PRF Pulse Repetition Frequency
PRS Position Reference System
RCS Radar Cross Section
RD RijksDriehoeksnetwerk

RPI Repeat Pass Interferometry

RWS Directorate General of Public Works and Water Management ('Rijkswaterstaat')

SAR Synthetic Aperture Radar

TAW ministerial Technical Advisory Committee for Water Defences ('Technische

Adviescommissie voor de Waterkeringen')

TNO-FEL TNO Physics and Electronics Laboratory

TUD Technical University Delft

V&W Ministry of Transport, Public Works and Water Management ('Ministerie van

Verkeer en Waterstaat')

Wwk Water defence act of 1996 ('Wet op de waterkeringen')

1. Introduction

In ground engineering the need for deformation measurements is urgent. SAR interferometry can be used to measure small (sub-wavelength, i.e. cm) deformations. An experiment to investigate this for dike deformations was set up. This report describes why deformation measurements are needed, part of the interferometric experiment and the first results. The remainder of the current chapter serves as an introduction to SAR interferometry in general.



Figure 1.1: The PHARUS SAR system used for this experiment. The radar pod is visible below the cockpit.

1.1 Motivation for the experiment

In ground engineering the need for deformation measurements of wide areas in density populated regions such as The Netherlands is urgent. Such information is necessary for large building sites and underground construction, like deep excavations and bored tunnels in soft ground in urban areas. Also for water defences, roads, and the monitoring of land subsidence due to water level control in polders and other long term monitoring of wide areas detailed information on deformations becomes necessary. Accurate deformation monitoring of larger areas, however, is time consuming and requires expensive efforts. Nevertheless, the sometimes important consequences of deformation in densely populated areas require such information to be available.

As a pilot for ground engineering the present project deals with water defences. The information obtained in the project is to support analysis of two aspects for which detailed information on deformations of river dikes is needed, notably:

- Monitoring of deformations during high water periods, which yields information on stability and possible failure mechanisms of dikes which is to be used in early alert decision systems, and
- Determination of long term settlements, which diminish the local dike height which is related to subsoil and hydrological conditions and therefore requires periodic surveillance.

During extremely high floods a dike can lose its stability, which can lead to catastrophic inundation of the polder to be protected. Loss of stability is warned for by increasing deformation of a dike. For an early warning system, which should support decisions to evacuate, input of actual information on water-levels and deformations is essential. Only remote sensing techniques can supply such information in an efficient way.

Substantial developments are foreseen for the coming years concerning the use of deformation data by authorities in The Netherlands responsible for safety evaluation of dikes during high river floods and for maintenance purposes. The ministerial Technical Advisory Committee for Waterdefences (TAW, 'Technische Adviescommissie voor de Waterkeringen') is incorporating the so-called "actuele sterkte" line of research concerning deformation analysis in the present planning period. In the recently prepared guidelines for evaluation of the safety of water defences [TAW, 1994] the necessity of systematic monitoring of deformation of existing dikes is stated. Such monitoring has not been common practice in general and will therefore entail a substantial increase in monitoring activity. SAR interferometry, which is capable of monitoring mm-level deformations, is the technique investigated in this experiment.

1.2 SAR Interferometry

SAR interferometry is a relatively new technique with a number of highly promising applications, amongst which:

- the creation of land surface deformation maps with extremely high accuracy
- the generation of high accuracy digital elevation models
- improved target recognition by creation of 3D images of targets
- improved land use classification by exploiting coherence measurements
- the measurement of current fields and moving target indication

In SAR interferometry the phase of the received backscattered signal is used to measure path length differences with mm accuracy between SAR images taken from slightly different positions or at different times. The path length differences can be related to important parameters such as the terrain height, the velocity of the targets and the deformation of the surface of the Earth.

Three types of SAR interferometry can be distinguished:

- repeat pass interferometry.
- across track interferometry
- along track interferometry

In repeat pass interferometry use is made of SAR images taken approximately from the same position at different times. This is the ideal situation for the measurement of deformation of the Earth's surface and for change detection. For across track interferometry the SAR images are acquired with the SAR antennas displaced in a direction perpendicular to the track of the aircraft or satellite. This is the optimal situation for measurement of the terrain height. Finally, in along track interferometry the antennas are displaced along the flight direction. In this way velocities of targets like cars or currents in the sea can be measured.

Because deformation measurements are the subject of this report, the next section provides more detailed information about especially this type of measurement.

1.3 Interferometric deformation measurements

One of the most promising applications of repeat pass SAR interferometry is the measurement of small surface deformations accurate to millimetre level. The SAR instrument is extremely sensitive to small relative changes in elevation occurring in the time interval between the passes. It allows rapid and precise determination of relative vertical and horizontal displacement. TNO-FEL, the Delft University of Technology and the Survey Department of Rijkswaterstaat have put considerable effort in the exploitation of this technique for the measurement of deformation caused by gas extraction in Groningen. The same technique can also be applied in other disciplines like geology for the monitoring of volcano's, the area extended monitoring of the effects of earth quakes and the measurement of the flow of glaciers. Figure 1.2 shows the principle of an interferometric deformation measurement.

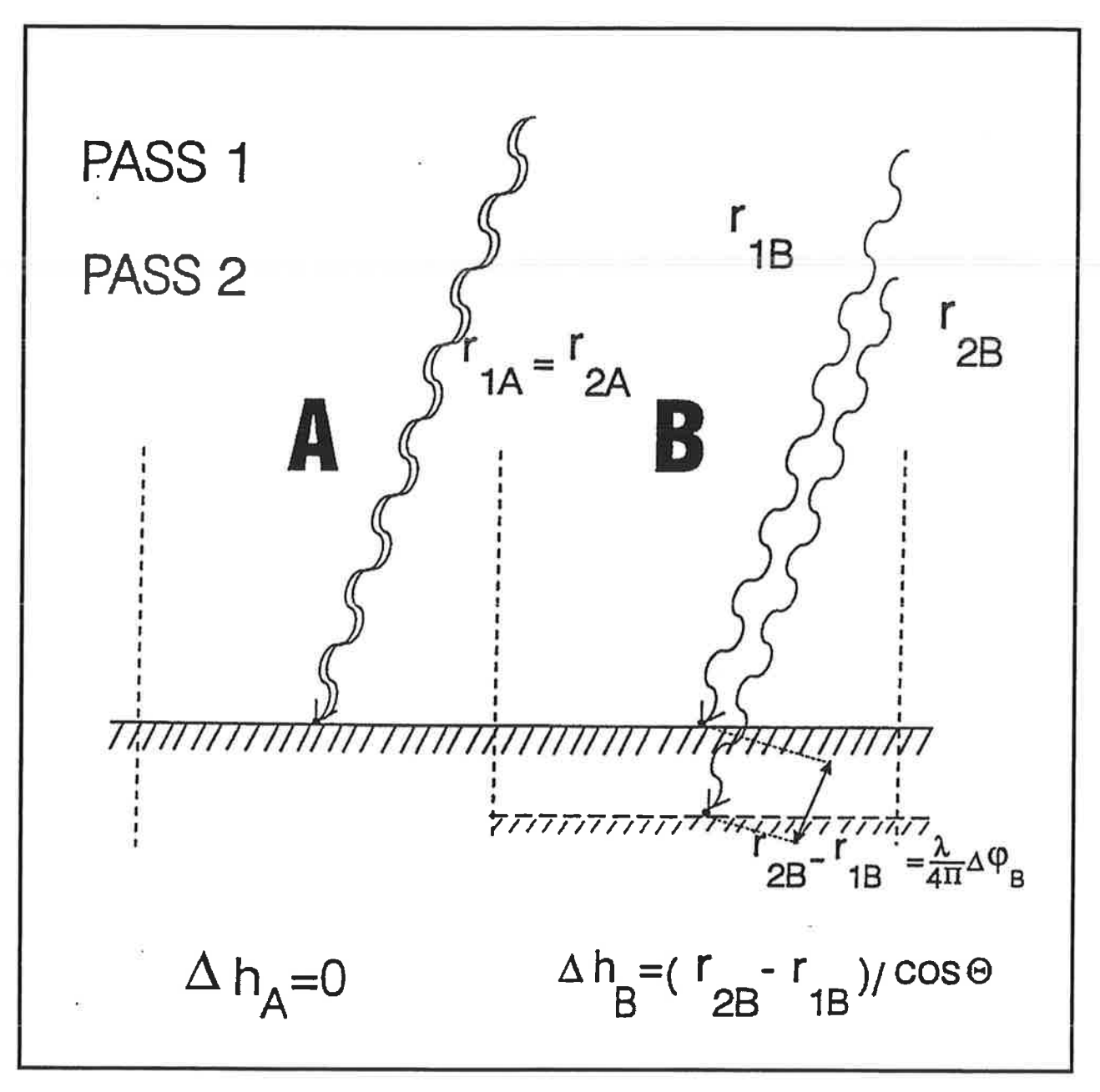


Figure 1.2: Schematic representation of the repeat pass deformation measurement principle.

Terrain A did not change in height (Δh_A =0) in between passes 1 and 2 (which are separated sufficiently in time for a deformation in the order of millimetres to occur). On the other hand, terrain B subsided a small amount Δh_B , which is related to the measured range difference through Δh_B =(r_{2B} - r_{1B})/cos θ . θ is the look angle (the angle between the vertical and the radar look direction). The primary parameter measured by a SAR is the phase, so the height change can be found with

$$\Delta h_B = \frac{\Delta \phi_B \lambda}{4\pi \cos \theta},\tag{1.1}$$

in which $\Delta \phi_B$ denotes the phase difference measured between pass 2 and 1. Because phase measurements can be accurate to within a few tenths of a radian, the subsidence exhibits mm level accuracy (assuming a wavelength λ =5.66 cm and a moderate look angle).

1.4 Contents of the report

The chapters of this report describe the following:

- 2. the deformation problem in detail, and the formulation of user requirements for a deformation measurement system (see also appendix A and B).
- 3. the requirements and preparations for orbit and beam direction control (see also appendix C), and the integration of DGPS and INS data. These are necessary for useful interferograms.
- 4. details of the interferometric experiment, like the test site location, ground equipment used, etc.
- 5. analysis of the flight lines, beam angles occurring during the flight, and of the SAR data (non-interferometric).
- 6. analyses of interferograms made with this data.
- 7. analyses of an interferogram computed from newer (3-2-2000) data, including the changes made to the processing software.

The results of the first flights (reported on in chapter 4-6) were disappointing due to several flaws in the data and processing software. The BCRS was asked for permission to postpone the publication of this report, in order to incorporate results of newly acquired data. Permission was granted and led to chapter 7, which presents improved results.

2. User requirements

2.1 Problem and objective

The problem in the present case is related to 3 topics in water defence management, namely:

- 1. Decision support for water defence and administrative management during extreme high water conditions.
- 2. Safety assessment of dikes every five years, as prescribed in the Water defence act of 1996 ('Wet op de waterkeringen'; Wwk).
- 3. Monitoring of the deformation behaviour of dikes.

Each of the aforementioned topics is discussed separately in the following three sections.

2.1.1 High water conditions

During the high water periods of 1993 and 1995 the strength of dikes was calculated using conventional methods. On the basis of these calculations various measures were taken. In spite of a calculated lack of stability of certain dikes, these withstood the high water level without noticed severe deformation or damage. The question was raised whether the methods used to calculate the stability of dikes were adequate.

During high water periods decisions were made on the basis of the aforementioned calculations and some were made on the basis of observations, such as signs of deformation of the dike or water appearing behind the dike. These observations were rather subjective. Visual observations cannot describe the magnitude of the deformations and water flow with sufficient accuracy.

There is a need for a system to measure deformation accurately and objectively at short notice and within a short time. Such a system could be very useful to support authorities in decisions during high water periods.

2.1.2 Safety assessment of dikes every five years

Since 1996, the Water defence act prescribes an assessment of the safety of each water defence construction every five years. At the moment the first assessment is being executed. The stability of some dikes is qualified as insufficient, although those dikes have withstood water levels higher than the current criterion. Again the question was raised whether the methods used to assess the stability of dikes is suitable.

In order to assess the safety of a dike both the actual height and strength of the dike have to be determined. In order to do so the height and geometry are to be measured. Conventional methods are time consuming and most methods only present local cross sections, which are considered

representative for a certain stretch of dike. The selection of these cross sections is presently based on a minimum of information.

With the introduction of the Water defence act a need arose for a system which measures the actual height and cross section of a dike continuously along a stretch at reasonable costs. Vertical deformation measurement could supply the necessary information.

2.1.3 Monitoring

In order to assess the safety of a dike accurately it is necessary to 'know' the dike. This knowledge can be gathered in three ways:

- 1. By studying the history of the dike. This information could lead to the conclusion that the dike might be stronger than follows from current calculation methods ('proven' strength).
- By assessing the strength of the dike using calculations. In these calculations many uncertainties have to be accounted for, which will then have to result in underestimation of the real strength of most dikes.
- 3. By extrapolating observed deformation behaviour to extreme conditions.

Each of these methods separately will not lead to an accurate estimation of the actual strength of a dike. A combination of the aforementioned methods can lead to a more accurate estimation of the actual strength. The use of the first and third mentioned method can lead to a reduction of the uncertainties in the second method. Therefore, monitoring the deformation behaviour of a dike can help 'understand' the dike better and can help to improve the methods to assess the safety of a dike.

In order to establish a monitoring program a flexible system is needed that is able to measure deformations of a distinct number of cross sections all over the land at a reasonable price.

2.1.4 Project 'Actual strength' ('Actuele sterkte')

In order to answer the questions raised and to provide a more accurate method to calculate the stability of existing dikes the project 'Actual strength' ('Actuele sterkte') was started in 1995 by the TAW. The objective of this project is to develop a method or methods to assess the stability of dikes more accurately than is possible using current methods.

In order to assess the safety of a dike accurately it is necessary to 'know' the dike as mentioned above.

2.2 Activities

In order to achieve the objectives mentioned above the following activities were carried out and reported, namely:

1. Compilation of types of dikes and terrain with regard to loading and influences on deformation (section 2.3).

- 2. Description of types of deformation (failure mechanisms) related to dike and terrain type, with emphasis on rates of deformation (section 2.4).
- 3. Consultation of available sources and 'Waterschappen' on requirements and current procedures (section 2.5).

The results are given in the remainder of this chapter.

2.3 Types of dikes, loads and subsoil

2.3.1 Types of dikes

In the Netherlands three types of dikes can be distinguished:

- 1. Primary water defences.
- 2. Secondary water defences.
- 3. Reservoir dikes.

2.3.2 Primary water defences

The primary water defences can be sub-divided into four categories:

- 1. River dikes in the area of the Netherlands without tidal influences (eastern part of the Netherlands).
- 2. River dikes in the area of the Netherlands with tidal influences (western part of the Netherlands).
- 3. Sea dikes (in the estuary region in the south-western part of the Netherlands, along the North Sea and the Wadden Sea).
- 4. Lake dikes (along the IJsselmeer, the Markermeer and the water between Flevoland and the main land).

The recent dikes frequently consist of a sandy core covered with a clay layer and grass or a hard revetment. In many cases there is a road on top of the dike. The somewhat older dikes dikes (before 1953) usually consist of clayey material only.

Because of stability reasons or danger for piping a verge ('berm') is frequently applied on the landward side of the dike.

These dikes are loaded by high water levels against the outside of the dike (river side), by waves, by rain infiltration or by traffic surcharges. All of these loading types are temporarily. A high water period can last for several weeks, but the peak will pass a river dike in only a few days.

2.3.3 Secondary water defences

Secondary water defences often are old primary water defences and not as high a the present water defences. The secondary water defences divide a polder in sections. If a dike breach occurs the closest section will flood first, creating time for inhabitants in other sections to be evacuated.

Because dikes are usually old dikes they consist of clay and clayey material only. A road is often present on top of the dike. These dikes usually have no verge, since they are not designed to withstand high loads.

Most of the time these dikes are loaded by a traffic surcharge only. In case of a breach of the primary water defences these dikes can be loaded by a high water level, which then can stay on for several weeks.

2.3.4 Reservoir dikes

A polder is enclosed by a reservoir canal ('boezem'). The water level in the canal is higher than the water level in the polder. The water level in the polder is maintained by pumping water out of the polder into the reservoir canal or by letting water in from the reservoir canal.

These dikes are loaded permanently by the controlled water level in the reservoir canal. Therefore there are only few uncertainties as to the loading.

2.3.5 Types of subsoil

In the coastal and peatland part of the Netherlands the immediate subsoil of dikes consists of peat and soft organic clay up to 20 meters thick. The thickness of these soft layers decreases towards the east until the subsoil consists of a thin clay layer on sand or just sand or gravel. Further eastwards and locally in the coastal area, sand subsoil is common.

2.4 Potential failure mechanisms

2.4.1 General

The potential failure mechanisms of dikes are schematically illustrated in Figure 2.1.

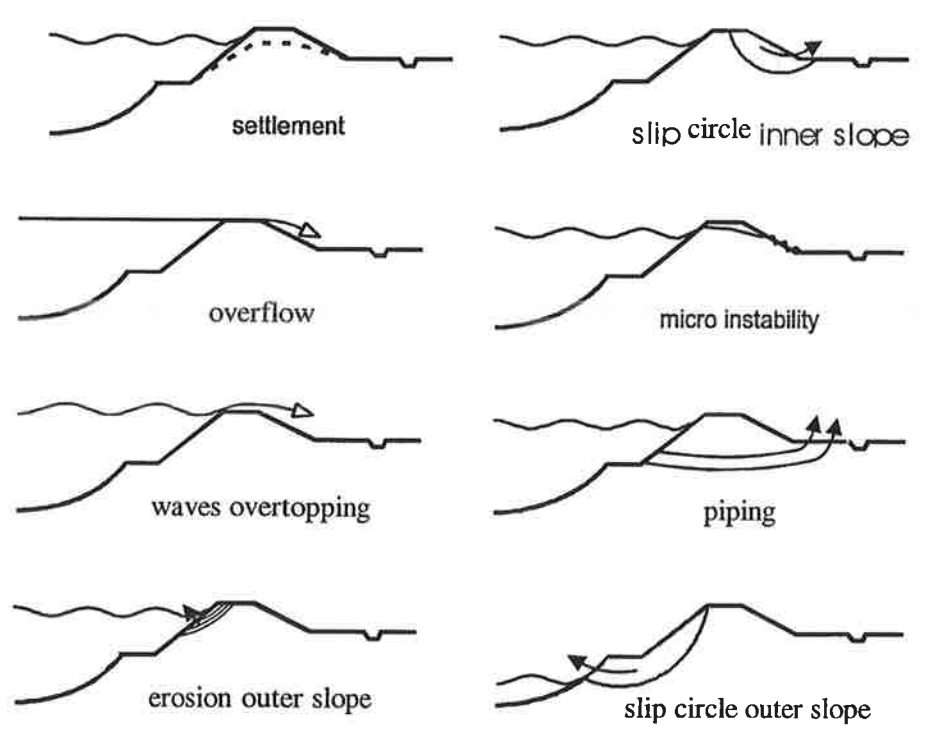


Figure 2.1: Potential failure mechanisms

In this chapter these failure mechanisms are explained, as well as the signs accompanying the mechanisms.

2.4.2 Settlement

The height of the crest of the dike decreases in time at a decreasing rate. For water defence management the height of the dike has to be determined regularly in order to check whether the dike still meets the demands.

It is evident that the settlement of a dike on a thick layer of soft soil will be larger than the settlement of a dike on stiff clay, sand or gravel. On soft soil settlements of several meters can occur during the life span of a dike. Most of the total settlement occurs in the first few years after construction, but settlement at a slower rate continues.

Settlement itself does not lead to failure of the dike. Differential settlements along a dike can be easily detected visually. Settlement is presently quantitatively determined using levelling techniques.

Measurement of the height of the dike is especially relevant for the safety assessment every five years and should be included in monitoring programs.

2.4.3 Overflow and waves overtopping

Overflow occurs when the water level in the river, or the water in waves, exceeds the crest of the dike. Overflow can result in inundation of the area enclosed by the dike directly, or indirectly by erosion of the crest and the inner slope or slipping of the top layer of the inner slope followed by failure of the dike.

Initially the phenomenon reveals itself by a thin layer of water on the crest of the dikes and water on the inner slope of the dike. This is usually detected by inhabitants or mobilised watchman ('dijkwachten').

This phenomenon occurs only during very high water levels.

2.4.4 Erosion of the outer slope

Water flowing along the outer slope, carrying all kinds of debris, and waves can affect the top layer of the outer slope. This may lead to erosion of the outer slope and subsequently decay of the dike.

This phenomenon is often not easily detected as most damage occurs just below water level.

2.4.5 Rotational slide inner slope

Loss of stability of the inner slope is considered a main failure mechanism, and can occur as water penetrates the core of the dike due to high river water levels. This soaking will take some time (mostly several days). The stability of the inner dike surface is undermined by the increased weight of the dike body and the decrease in strength of the soil due to excess waterpressures. So, during high water conditions the driving force will increase and the resisting force will decrease.

This phenomenon is not easy to observe visually, as initially deformations are only centimetres and cracks are being initiated. Loss of stability can occur at a deformation of a few centimetres for a stiff dike on a stiff subsoil, whereas deformation of 10 cm or more may not lead to loss of stability for a clayey dike on a soft subsoil.

Rotational slides usually only happen during high water periods or after a period of intense rainfall.

2.4.6 Rotational slide outer slope.

When the river water level drops fast (several meters in only a few days) the phreatic water level in a dike cannot follow the decline in river water level. The water pressure in the dike may then cause failure of the outer slope along shallow circular slip surfaces, or planar slides of liner material. The above mentioned failure of the outer slope happens rather fast and part of the slip surface will be under water and can therefore not easily be detected.

These failures happen when the river water level falls. Failures like this do not necessarily result in complete failure of the dike and subsequent inundation of the enclosed area.

2.4.7 Micro instability

Water flowing through the dike can surface somewhere on the lower half of the outer slope. This water can carry material from the top layer or the core, resulting in erosion of the inner slope. If noticed in time, countermeasures can be taken effectively. Some local deformation can be expected to be associated with this phenomena, related to small scale failures and quasi elastic behaviour of surficial dike material becoming saturated.

This phenomenon can happen as a result of a high water level in the dike.

2.4.8 Piping

A high river water level, and a much lower, controlled water level in the polder, causes water flow through permeable layers under the dike. This water surfaces at some distance behind the dike.

Upon high gradients, the water flow can carry grains from the permeable layer to the surface, creating small sand craters. The extrusion of sand grains from the permeable layer will cause a tunnel or pipe to develop which eventually undermines the dike.

The first sign of such a failure mechanism developing is water surfacing behind the dike. Later on a small sand crater may develop. This is a definite indication of a pipe developing, and for remedial measures to be taken.

The developing sand craters are submerged, and can be spotted by inhabitants or watchman ('dijkwachten') which make regular inspection rounds.

2.4.9 Summary

2.4.9.1 Deformations

The deformation of dikes comprises (quasi-) elastic and irrecoverable strain, some of which may give rise to failure of the dike. The relation between the load upon the dike and the strain can give information on the nature of the deformation. The occurrence of settlements and deformation such as initial creep movement preceding development of slip surfaces at the inner and outer slope can be detected by observing deformations.

The settlement rate is usually very slow: one or several centimetres per year after initial settlement has taken place. Measurements every few years can sufficiently well describe the deformation for maintenance purposes. These measurements can also provide information on the nature of the long term deformation (vertical and lateral components).

Monitoring deformation at regular intervals upon high river floods can indicate dike sections with abnormal or suspect deformation behaviour.

The deformation rate of a developing slip surface at the inner slope is moderately fast for geotechnical notions: a slip surface will develop in a matter of days. In order to monitor such detailed features, observations have to be made every few hours to once every day.

The deformation of a developing slip surface at the outer slope can take days to several hours. Deformations preceding such failures may well be noticeable if quantitative data would be available.

2.4.9.2 Surfacing water

Surfacing water itself is not a threat: usually it concerns only rather small amounts of water. In case of a pipe developing under the dike the appearance of a small (1 - 2 meter diameter) sand crater can be noticed.

2.5 Questionnaire

In order to investigate the applicability and need for an airborne SAR interferometric system for use for water defence management a questionnaire was drawn up and sent to representatives of several water boards. Since airborne SAR interferometry may offer possibilities for road maintenance and management, one questionnaire was send to an advisor for road design and maintenance. The questionnaire is included in appendix A (in Dutch).

Five responses were received: four from representatives of water boards and one from the advisor for road design and maintenance. An overview of these responses is given in appendix B (in Dutch).

From these responses it can be concluded that such a system can definitely be very useful for water defence management. However, for the system to be useful, some conditions have to be met:

- The system has to able to measure settlements and deformations of 1 to 3 cm with an accuracy of about one centimetre.
- The system has to be sufficiently available.
- During high water periods the system has to be made available at a few days notice and the results of the measurements have to be made available well within one day.
- For monitoring the deformation behaviour of dikes the system has to be available at least about once a year for measuring deformations of a certain dike sections on specific locations in The Netherlands.
- For safety assessment of dikes the system has to be available once every five years for measuring deformations of all dikes in the Netherlands.
- During high water periods the results have to be made available within about half a days time.
- For monitoring of the deformation behaviour of dikes and for the safety assessment every five years the results have to be made available within one month.
- The results of the measurements have to be made available in a suitable format for computer processing. From the responses to the questionnaire it is clear that there is not yet a standard for such a digital format.

From the response of the road design and maintenance advisor it can be concluded that an airborne INSAR system can be very useful for road management. Especially during the reconstruction of an existing freeway. The possible use of an airborne INSAR system for road management has to be investigated further.

2.6 Comparison of airborne InSar measurement with conventional techniques

InSar deformation measurements have potentially certain benefits which can hardly be attained with conventional techniques. Airborne InSar measurements can provide sufficiently detailed information at relatively very short notice under harsh ground conditions. The technique can also provide a surface coverage not reasonably possible with conventional techniques, and allows for much more detailed and in depth analyses of causes of deformation and any remedial measures. Presently used analyses techniques require a substantial amount of "experience" to come to reasonable evaluations of any measures to be taken, and where these measures are to be taken exactly.

Presently InSar deformation measurements are the only available technique that provides accuracy comparable to conventional levelling used for dike construction and maintenance. The cost of providing the information of InSar deformation measurements with conventional techniques would be extremely high to provide the density of information. Any comparison of costs of techniques will have to take the shortcomings and benefits of each into account and will have to evaluate their effect on design, maintenance and emergency situations. The InSar system has a very high potential in improving the practice.

3. Experimental considerations

Repeat pass interferometry with spaceborne SAR systems like the ERS-2 is nowadays performed more or less routinely. The main reasons are the good stability of the radar as well as the repeatability of the satellite's orbit and attitude¹. Interferometry with airborne systems is more difficult, because orbit and attitude control are more difficult due to the atmosphere. Nevertheless, airborne interferometry was demonstrated in [Gray and Farris-Manning, 1993], [Ulbricht and Reigber, 1998] and [Miyawaki *et al.*, 1998]. The demands of airborne RPI and our precautionary measures taken to enable measuring good quality interferograms are the subject of the following.

3.1 Orbit and beam direction conditions

The orbits and attitudes related to two SAR images have to satisfy two conditions for a quality interferogram. These conditions are quantified in the next two sections.

3.1.1 Perpendicular baseline condition

If the incidence angles of the two passes (for a single resolution element) differ too much, no coherence results. If the absolute value of the perpendicular baseline (directly related to the incidence angle difference) exceeds the critical perpendicular baseline [Zebker and Villasenor, 1992], no coherence can be obtained:

$$B_{\perp,critical} = \frac{\lambda r \tan \theta}{2\rho_r}, \text{ with}$$
 (3.1)

 $B_{\perp,critical}$ critical perpendicular baseline [m]

 λ wavelength [m] r slant range [m]

 θ incidence angle [deg]

 ρ_r slant range resolution [m]

In our case we have typically $B_{\perp,critical} \approx (0.0566 \times 12000 \times \tan(60^\circ))/(2 \times 3.4) \approx 173$ m (this corresponds to an incidence angle difference of $(180 \times 173)/(\pi \times 12000) \approx 0.83^\circ$). The loss of coherence is due to the radar seemingly observing slightly different objects at different incidence angles (just like an ordinary car looks different from different aspects). The spectral interpretation is that the object spectra do no longer overlap if the baseline exceeds the critical value [Gatelli *et al.*, 1994].

I Conventional radars (like ERS) use antennae of which the direction is fixed with respect to the fuselage. The antenna direction can only be changed by changing the aircraft's attitude. Phased array antennae (like PHARUS uses) can change the direction electronically, independent of the aircraft attitude. In interferometry (relative) azimuth antenna directions are important, not attitudes.

3.1.2 Azimuthal beam difference condition

The difference of the (horizontal) azimuthal beam directions of the two passes, $\Delta \varphi$ [deg], should fulfil the following inequality:

$$\left|\Delta\varphi\right| < \frac{90\lambda}{\pi\sin\theta\rho_{c}}$$
, with (3.2)

 λ wavelength [m]

 θ incidence angle [deg]

 ρ_a azimuth resolution [m]

In fact, if equality holds, no coherence between the two images remains. Again, the loss of coherence is due to the target "looking differently" from different azimuthal angles. The spectral interpretation is now that the Doppler spectra do no longer overlap if equality holds for Eq. (3.2) [Geudtner, 1995]. In our case $\Delta \varphi \approx (90 \times 0.0566/(\pi \sin(60^\circ) \times 1) \approx 1.9^\circ$.

Assuming a linear, multiplicative model, we can write

$$\rho \approx \left(1 - \frac{\left|B_{\perp}\right|}{173}\right) \left(1 - \frac{\left|\Delta\varphi\right|}{1.9}\right) \rho_{r} \qquad \text{(for } 0 < \left|B_{\perp}\right| < 173, \ 0^{\circ} < \left|\Delta\varphi\right| < 1.9^{\circ}; \ 0 \text{ otherwise)}$$
 (3.3)

for the measured coherence of an object with real coherence ρ_r . If we allow for a coherence loss of at most 10 % due to baseline and 30 % due to azimuthal difference effects (totalling 37 % loss), we obtain the following approximate conditions:

- B_⊥<20 m
- Δφ<0.6°

For a single pass the aircraft position should therefore be within about 10 m of a planned flight track, while the beam azimuth should deviate from it by less than 0.3°. The following section describes how this could be achieved.

From a spectral point of view, a small coherence is due to the small overlap of the spectra of the master and slave images (in range and/or azimuth). By filtering the none-overlapping parts the coherence increases. However, at the same time the resolution of the interferogram degrades, because the filtering operation decreases the bandwidth.

3.2 Orbit and beam direction control

3.2.1 Real time orbit control with DGPS

Orbit control of PHARUS is normally done with a GPS (Global Positioning System) and (pressure) height sensors. In combination with the auto-pilot of the Citation this leads to orbit repeatability

accuracies of up to hundreds of meters. This is not sufficient for interferometry. The 10 m condition was planned to be met by using the NLR developed PRS (Position Reference System), of which the information was fed into the auto-pilot. The accuracy foreseen was about 1 m. To be able to fly with this precision, the PRS had to be set to the code-tracking differential mode. This mode requires a ground-based reference station close to the operating area of the aircraft. The reference GPS data is sent to the aircraft by means of a telemetry uplink, where in real time an orbit is calculated with ≈ 1 m accuracy.

The PRS configuration in the aircraft consists of another GPS receiver, the telemetry input from the ground-based GPS and an IRS (Inertial Reference System), all connected to the VME-based PRS computer. The PRS computer is running a real-time Kalman filter to obtain the best possible aircraft position.

The differences between a pre-defined track and the calculated aircraft position are converted to a suitable format for connection to the auto-pilot of the aircraft, resulting in horizontal and vertical guidance of the aircraft. The auto-pilot needs to be in landing mode for correct operation. A block diagram of the hardware in use is given in Figure 3.1.

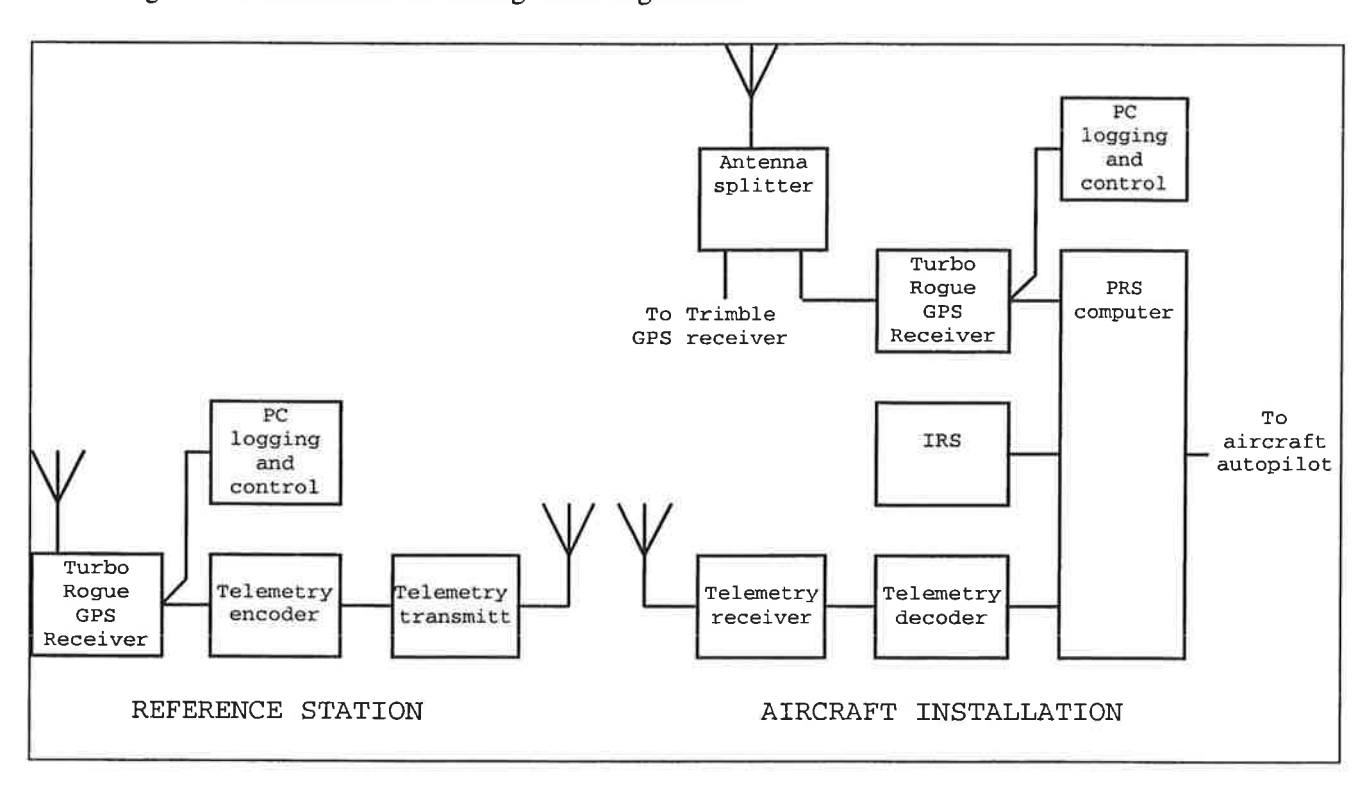


Figure 3.1: Block diagram of navigation hardware.

After a first test flight (performed on 11-9-1998) it was obvious that the autopilot correction signals were not properly matched to the aircraft dynamics at the height and speed it was required to operate. After a change in some calculation parameters a second test flight (21-10-1998) was performed where sufficient guidance for the experiment was shown.

3.2.2 Beam direction control

In order to fly the required flight track under all wind conditions, the attitude of the aircraft changes in response to the auto-pilot generated steering command. Therefore, to approach the requirement of $|\Delta \varphi| < 0.6^{\circ}$ antenna beam steering had to be used to point the antenna correctly at the observation area. The beam direction of the phased array antenna of PHARUS can be steered electronically in the slant range plane, in 0.5° steps. By using (in-flight available) orbit and attitude data it is possible to point the beam in the desired direction. Prior to the RPI experiment two beam steering modes existed:

- 1. "fixed beam steering": just before radar data collection starts the main beam direction is (electronically) steered to the direction perpendicular to the velocity vector. During the datatake the beam direction is not changed anymore. The result is a Doppler spectrum that is at first centred around zero Doppler. If the aircraft attitude changes the spectrum shifts from zero-Doppler, and can even move outside the sampled bandwidth.
- 2. "active beam steering": during the radar data collection the main beam direction is steered every second towards the direction perpendicular to the instantaneous velocity vector.

Beam steering mode 1 nor 2 do provide the earth-fixed beam direction required for RPI: in mode 1 the beam direction moves unpredictably with the aircraft's attitude. In mode 2 the beam is always oriented perpendicular to the velocity. However, the velocity direction is not fixed. Therefore, the beam direction also varies unpredictably. Therefore we introduced beam steering mode 3, especially suited to the needs of interferometry

3. "geographical beam steering": the beam is pointed (every second) in a specific horizontal direction (perpendicular to the ideal flight track), fixed with respect to the geographical north.

Only with this third mode it is possible to approach the required small azimuthal beam variation. Appendix C discusses the beam steering modes in some more detail and presents data of the "geographical beam steering" mode obtained during a measurement flight.

3.3 GPS processing for high accuracy off line orbits

3.3.1 Trimble GPS and associated software

As mentioned in section 3.2.1, a Turbo Rogue receiver was used for real time navigation in DGPS mode (by means of code corrections transmitted to the aircraft by a data link) with an accuracy of about 1 m. To aid off line motion compensation by (i.e., by providing a precise orbit to the SAR processor), another GPS receiver (brand: Trimble 4000 SSi) was mounted in the aircraft, in addition to the Turbo Rogue receiver. The data of the Trimble eventually resulted in a high precision (<10 cm) flight-track (sampled at 1 Hz). Both receivers were connected to the same Dorne Margolin antenna by means of an antenna splitter. Unfortunately, the signal strength for the Trimble receiver was in this way only just sufficient, [de Jong and Jonkman, 1999]. The equipment in the aircraft is shown in Figure 3.2.



Figure 3.2: The equipment in the aircraft (the Trimble 4000 SSi receiver is at the upper-left side)

The ground-based reference receivers were of the same type as those in the aircraft, i.e. one Turbo Rogue and one Trimble. The Trimble receiver was connected to its own Geodetic L1/L2 antenna. The location of these ground stations was selected to be as close as possible to the flight tracks. The WGS-84 co-ordinates of both ground stations were determined with a precision of 1-2 cm. The ground station set-up is shown in Figure 3.3. The measurements were carried out during a good satellite configuration when a sufficient number of satellites (≥ 5) was available with a good geometry (PDOP < 6) for an elevation mask above 15° .



Figure 3.3: Set up of the ground stations in the neighbourhood of Herwijnen.

The postprocessing of the Trimble data was carried out using double difference carrier phase observables² [Hofmann-Wellenhof, 1997; Teunissen and Kleusberg, 1998]. As a result, the clock errors of receiver and satellites are eliminated. By using L1 en L2 data the ionospheric influence could be removed. The solution thus obtained is referred to as an ionosphere free solution. The ambiguities in the phase observables were resolved using an "On The Fly" (OTF) method. If the integer values of the ambiguities can be determined, the solution is referred as ionosphere-free fixed solution, if not, it is called an ionosphere-free float solution. The fixed solution is the better of the two, with precision of the order of several cm.

In order to obtain the best positions by postprocessing, the software packages GPSurvey, GeoGenius and Flykin were tested and the results compared using a test dataset. The differences between these packages apply to:

- The possibilities for input and output data
- Number of options for the data processing
- The maximal range for ionospheric free fixed solution
- The computed positions (!)
- Quality control and quality indicators
- User friendliness.

GPSurvey (version 2.3a) is a product of Trimble, USA. The advantage of this package is the great reliability in the position solution, even over greater ground station to aircraft distances. The disadvantages are the long computing time and the poor information in the kinematic output file. This file contains only GPS-time and WGS-84 positions (latitude, longitude and height), but no quality indicators. In addition there is no information about the ambiguities in the phase-observables. Extra information is given in a report file, including a graphical presentation of the residuals (also per satellite) after the adjustment. The residuals are very useful for quality control.

GeoGenius (version 1.6) is a product of Spectra Precision Terrasat GmbH, Germany. The input and output are presented in an excellent way. The kinematic output gives also information about standard deviations, number of satellites and PDOP value for each epoch. Much information is given in a separate report file, also on the ambiguities. The disadvantage of this package is that the maximum ground station to aircraft distance for resolving the carrier ambiguities is restricted to about 20 km.

Semikin-Flykin (a new version is called Flykin Suite) is a product of GEOsurv Inc., Canada. Initially there were many problems with this package and the results were disappointing [Husti and Sluiter, 1998]. After intensive communication with GEOsurv a more useful new version was obtained in January 1999. In spite of the improvements the drawbacks of this new software package are:

• there is no option for ionosphere free solution (this option is needed with ranges greater than 5 km);

² This means that first the single differences between the phase observables measured by two receivers were computed, and then the double differences between the single differences of two satellites.

- resolving the ambiguities is only possible forwards or backwards (but the two solutions are not always the same!) and there is no option available for an optimal ambiguity solution like there is in other software;
- maximum distance for resolving the carrier ambiguities is restricted to about 20 km while in some cases the positions were not correct even for shorter distances.

After comparison of the three software packages we arrived at these conclusions:

- GPSurvey supplies in general the best results;
- the position differences between GPSurvey and GeoGenius are in most cases a few centimetres (thus negligible);
- Flykin Suite was not useful for this project and should be improved.

3.3.2 Integration of Trimble GPS and IRS data

Due to the fact that phase-differential instead of stand-alone GPS had been applied (the accuracy of phase-differential GPS is expected to be at the centimetre level), modifications of the PHARUS trajectory-software were required. A flow-chart of the software after the modifications is given in Figure 3.4.

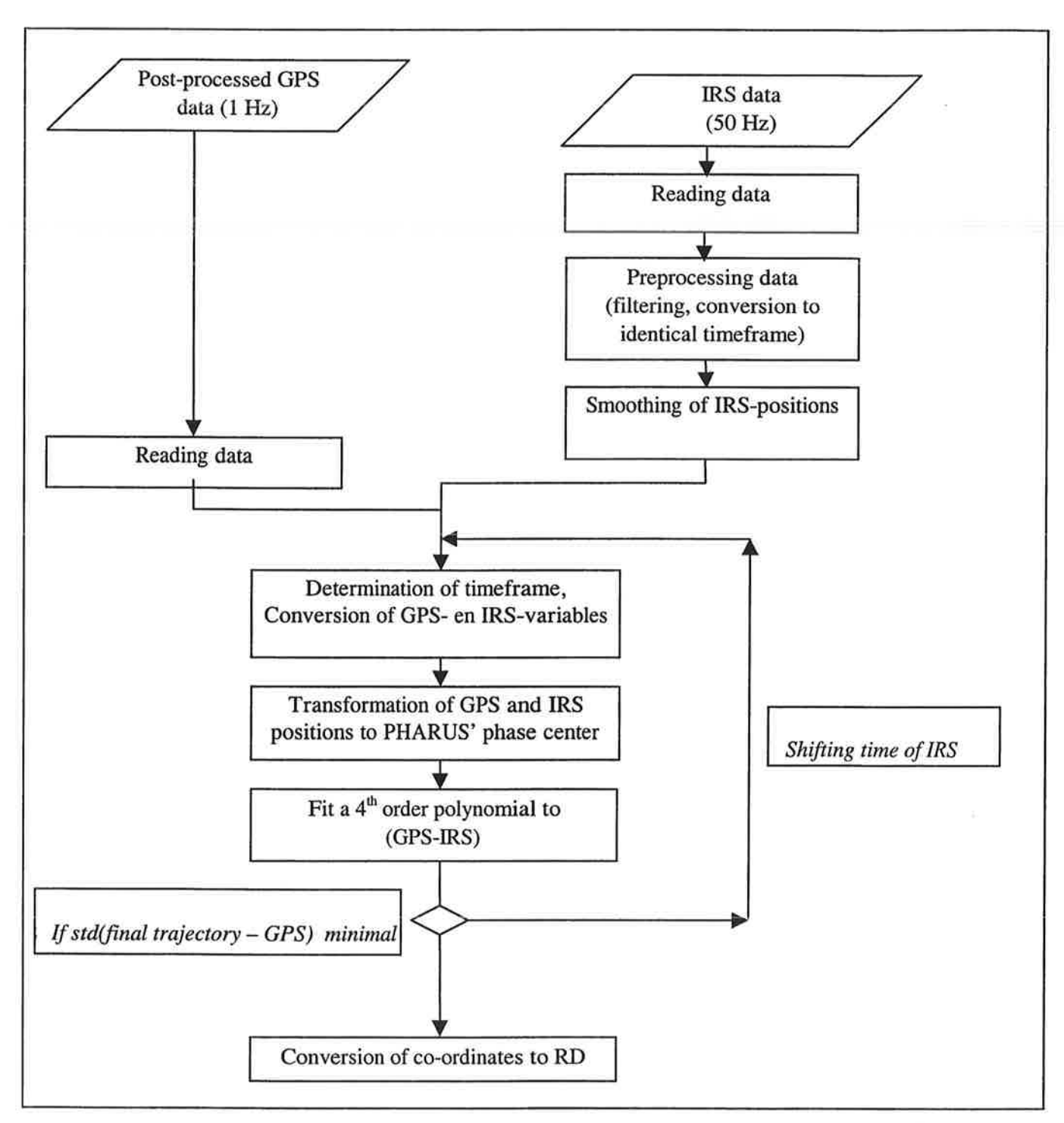


Figure 3.4: Flowchart of the PHARUS trajectory software. The 'final trajectory' is the sum of the 4th order polynomial and the IRS trajectory.

It is necessary that the final result, obtained using GPS as well as IRS (Inertial Reference System) as input, is becoming more depending on GPS when using phase-differential processed data. The tuning of this dependence in the software is performed as follows. A polynomial is estimated between the

difference of the GPS and IRS results. Good focusing of the SAR imagery was obtained with a fourth order polynomial.

A second modification is the transformation of the GPS and IRS coordinates to the phase centre of the PHARUS antenna. This step has become necessary due to the strict requirements with respect to accuracy. The transformation is performed using the location of the sensors on the aircraft as well as the angles measured by IRS.

The last modification was the determination of the error of the time-values of the IRS. This error has to be determined since it has an impact on the final results (i.e. the trajectory). Determination of this error and the corresponding trajectory is performed as follows. The complete trajectory is computed several times, each time a specific small shift of the time-values of the IRS has been applied. The shift that yields the smallest residues (sta(final trajectory - GPS)) results in the most optimal trajectory.

4. The experiment

4.1 Location

A dike near Gorinchem (The Netherlands) was selected in co-operation with the Hoogheemraadschap as the main target of the INSAR measurement flights with PHARUS (Figure 4.1). This dike deforms rapidly. For example, it subsided at a rate of 1.2 cm per month between September 1998 and January 1999. Figure 4.1 shows a topographic map and a photograph of the dike and its surroundings.





Figure 4.1: Topographic map (with Gorinchem at the right and the dike at the left) and photograph of the dike and its surroundings.

The dike is indicated at the left on the topographic map. Part of it is oriented north-south (approximately), part of it West-East. The RD coordinates of our aiming point on the dike are (122930,427783).

Figure 4.2 gives a cross section of the subsurface of the dike, showing it is build in a terrain underlain by thick peat and soft clay deposits whose low strength and high compressibility explain the observed high settlements after the improvement of the dike in the past year.

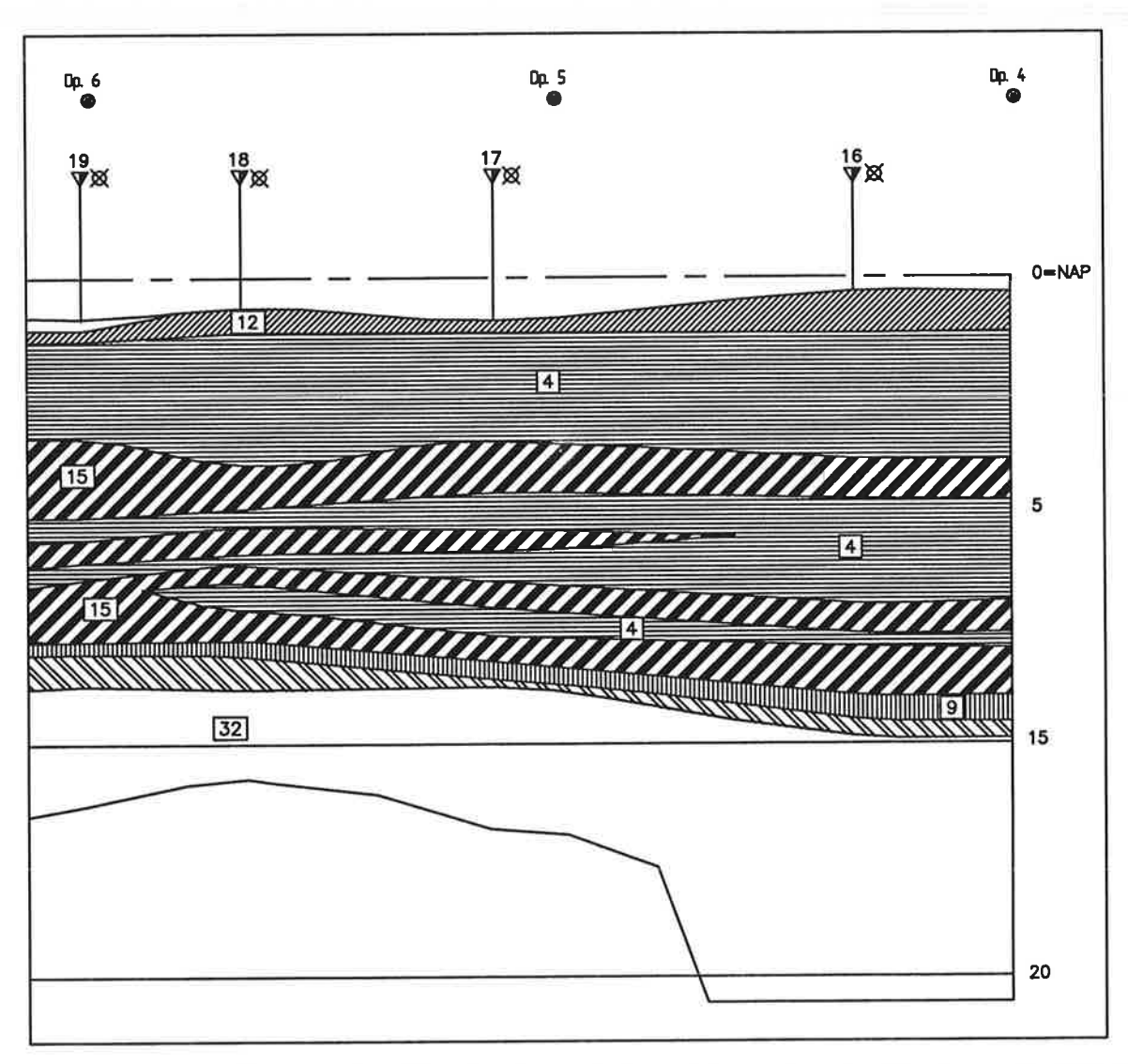


Figure 4.2: Geotechnical profile of the subsurface in the immediate vicinity of the dike, showing the thick clay and peat deposits whose low strength and high compressibility cause the observed strong deformation. Explanation: Inverted triangles and circles = CPT and borehole; 12 = clay; 4 = peat; 15 = organic clay (flood basin deposits); 9 = basal peat (transgressive); 32 = Sand (Pleistocene).

4.2 Corner reflectors

Eight square based corner reflectors were deployed as stable phase references (Table 4.1).

Table 4.1: Corner reflector details. The size refers to the side of the square base. The RCS is valid at C-band (5.3 GHz). The azimuth is the angle between the geographical north and the boresight direction, measured clockwise. The elevation is the angle between the horizontal and the baseplate.

number of reflectors	size [m]	boresight RCS [dBm²]	azimuth [deg]	elevation [deg]
4	0.65	26.8	138	1.4
4	0.93	33.1	138	1.4

The reflectors were deployed in three groups (Figure 5.6). The northern group of 4 reflectors (two small and two large ones) were spread out across the dike slope, down to the lowest land. In this way it was expected to be possible to measure the phase of the moving dike reflectors with respect to the phase of the stable lower ones. The other four reflectors were deployed in two groups of two, also close to the dike and farther away.

The 138° azimuth points exactly halfway between the 33° and 63° track angles. This (33+63)/2-33)=15° azimuthal deviation from boresight causes a decrease in the RCS. Due to the broad RCS pattern of the reflectors, this is only 2.1 dBm².

The corner reflectors were each mounted on 3 ground anchors with a diameter of 132 mm and a length of 400 mm. The anchors were fixed at about 0.3 m below the groundsurface and were fitted with a screw-thread, enabling exact re-placement of the reflectors in subsequent surveys. The depth of the ground anchors was chosen so as to adequately represent the relevant movement of the soil on the steep slopes (1:2.5) of the dikes (i.e., not the surficial movement, or dike independent movement of the anchoring system). The set up of the reflectors with these anchors allows for removal of the anchors between surveys, while guaranteeing representative displacement.

A word about the choice of reflector sizes is in place here. The phase of a reflector as determined from SAR imagery depends on its surroundings. That is because the power backscattered by the background present within the reflector resolution cell adds in an unpredictable way to the reflector power. The maximum phase error is given by

$$\alpha = \arcsin\left(\sqrt{A} \times 10^{\frac{\sigma^0 - \sigma_c}{20}}\right), \text{ with}$$
 (4.1)

 α phase error [deg]

A ground resolution cell area [m²]

 σ^{ρ} background backscattering coefficient [dB]

 σ_c corner reflector RCS [dBm²]

The formula shows that the error increases with increasing resolution cell size and background backscattering coefficient, and decreasing reflector RCS. The ground resolution cell of PHARUS is at least about 5 m². Figure 4.3 shows the maximum phase error for a range of background backscattering coefficients and reflector RCS's.

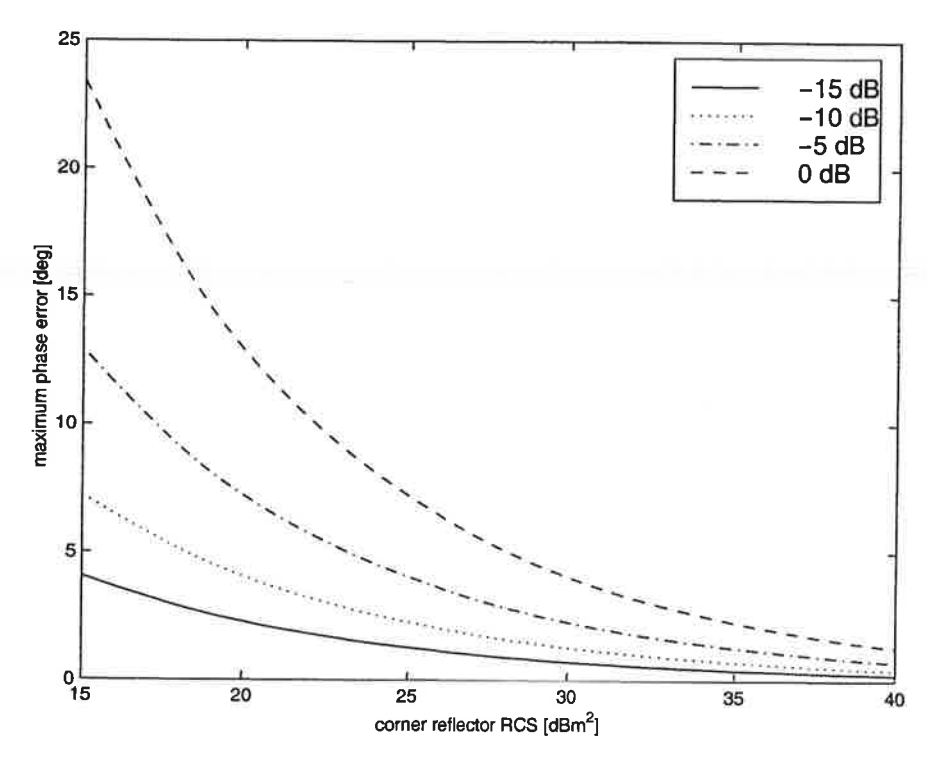


Figure 4.3: Phase errors due to the background, for background backscattering coefficients of -15, -10, -5 and 0 dB.

If one wishes to measure a dike deformation with 2 mm accuracy (with two images), the phase error should be below $180/\pi \times 4\pi\cos(60^\circ)/(0.0566\sqrt{2})\times 0.001\approx 5^\circ$. From the figure it follows that for a -15 dB background every reflector size plotted suffices. For -10 dB the reflector RCS should exceed 18 dBm², for -5 dB 23 dBm², and for 0 dB 28 dBm². Our reflectors (Table 4.1) meet this criterion (also if the 2.1 dBm² off-boresight loss is taken into account) for the most realistic background backscattering coefficient of -5 dB.

One, unknown reflector had an additional purpose: it was changed in height by some amount not known to the people analysing the data. This enabled a check of the entire processing and data interpretation chain. A correct retrieved height change would be indicate a successful experiment.

4.2.1 Corner reflector levelling

A levelling experiment was conducted with the purpose to determine the height of the corner reflector phase centres within the NAP system. The set-up of each levelling experiment is to establish local support points for a group corner reflectors. The initial idea is to connect the support points to nearby NAP reference markers. The height of the corner reflector phase centre is then derived from the local support points.

Purpose of the local support points is to reduce surveying time to establish the corner reflector phase centre heights. During a flight experiment, of which 3 were foreseen, one only needs to connect the corner reflector height to the local support point and not the NAP reference marker.

However, this generated an unanticipated problem in preparation for the postponed first flight on 9-sep-1998 when the support points showed an unacceptable height change compared to the heights observed on 4-aug-1998. To avoid this problem a full survey of all points was required. Therefore during the second flight experiment on 29-jan-1999 all support points, corner reflectors and NAP reference markers were used in the survey.

The results of three levelling activities are summarised in Table 4.2 showing the observed NAP heights for all points, markers, and reflectors. Points 67 and 70 are NAP reference markers, points 100 till 500 are local support points and 30005 till 60004 are the corner reflector phase centres.

Table 4.2: NAP observed heights of markers, support points and corner reflector phase centres on 3 dates. The columns labelled Diff 1 shows the height differences between 29-1-99 and 4-8-98, Diff 2 shows the height differences between 29-1-99 and 9-9-98. Note that the heights of the corner reflector phase centres between 9-9-98 and 29-1-99 are unrelated because of redeployment of the reflectors.

	0.1.00.00	00.00.00	20.01.00		77.1.000	
no.	04-08-98	09-09-98	29-01-99	Diff1	Diff2	Remarks:
70	5.7424		5.7424			NAP-marker
67	4.5741		4.5761	-0.0020		NAP-marker
100	6.7793	6.7782				
101	3.2782					
200	4.3326					
201			4.3403			
202			4.1521			
300	6.0883		6.0291	-0.0592		
301	2.8807	2.8732	2.8404	-0.0403	-0.0328	
400		3.4020	3.3990		-0.0030	
500		2.9704	2.9432		-0.0272	
30005		6.325	6.282			
30006		4.682	4.706			
30007		1.012	0.960			
30008		0.753	0.811			
60001		5.739	5.735			
60002		5.343	5.302			
60003		1.590	1.560			
60004		1.083	1.176			

Support points 100, 101, 201, and 400 are located in the neighbourhood of the northern group of 4 reflectors (dike pole 3) while 300, 301 and 500 are used for both south-western groups. The table shows that some support points are not present on 29-jan-1999 due to road construction activities in the area. New support points were installed to replace the old ones.

Remarkable are the height differences for support points 300, 301 between levelling experiment 3 on 29-jan-1999 and 1 and 2 on 4-aug-1998 and 9-sep-1998 respectively. It shows that the south-western part of the Wolpherense Dijk subsides as much as 6 cm in a time period of 5 months, roughly 1.2 cm per month.

4.3 Flight lines

Considerable care was taken in choosing the flight tracks (compare the tracks actually flown, plotted in Figure 5.1). The final choice is given in Table 4.3.

Table 4.3: Flight line characteristics. The track angle is the angle between the geographical north and the track (measured clockwise). The incidence angle is the angle between the vertical and the line of sight to the dike upon nearest approach.

flight line	begin RDx,Rdy [m]	end RDx,Rdy [m]	altitude [m]	track angle [deg]	incidence angle [deg]
1	130147, 419817	134504, 426526	6000	33	60
2	125198,417276	132326,420907	6000	63	60

4.4 Radar mode

The radar was operated in a mode of which some key parameters are listed in Table 4.4.

Table 4.4: Radar mode

parameter	value
polarisation	VV
presum factor	4
PRF	4000 Hz
range sampling frequency	100 MHz

4.5 Flights performed

In the second half of 1998 and the beginning of 1999 RPI flights were performed on:

•	11-9-1998	flight without radar, to test and improve the navigation
•	21-10-1998	idem
•	29-1-1999	flight with complete setup (radar and navigation equipment)

On other occasions a planned flight could not be carried out, due to radar failure³, auto-pilot problems⁴ or bad weather conditions. Especially the latter occurred frequently in January, i.e., icing conditions (the risk of accumulating ice on the aircraft)⁵. The measurement flight of 29-1-1999 (the only one providing radar data) consisted of the runs of Table 4.5.

³ The cause of this problem, a leak in the cooling system, was repaired.

⁴ It took some time before the combined DGPS/auto-pilot system functioned properly.

⁵ Measures can be taken to prevent ice accumulation.

Table 4.5: Data about runs.

run number	beam steering mode	track angle [deg]	start of recording [hh:mm] (local time)	remark
1	fixed	33	10:38	
2	geographical	33	-	orbit deviation up to 200 m
3	active	33	11:29	
4	fixed	33		orbit deviation up to 180 m
5	geographical	33	11:58	
6	fixed	63	12:12	
7	geographical	63	12:24	
8	active	63	12:37	
9	fixed	63	12:50	
10	geographical	63	13:03	

Although the "geographical" beam steering mode is most suited for interferometry (section 3.2.2), all three modes were planned to be tried. On the one hand because the differences between them would be interesting, on the other hand because the newly implemented "geographical" mode was never tested. The corner reflector was planned to be moved between run 3 and 5, as described in section 4.2.

During runs 2 and 4 the orbit was not close enough to the planned track to be of use for interferometry. The remaining 8 runs yielded useful radar data.

5. Basic data analysis

5.1 GPS orbit data from phase measurements

The first data available from the experiment were the GPS positions measured by the Trimble 4000 SSi receiver and processed by the software package GPSurvey (section 3.3). A reference station was positioned in the neighbourhood of Herwijnen. The data consisted of RDx, RDy and height values at a frequency of 1 Hz, with an accuracy of better than 10 cm. The projected flight track of the aircraft at 6 km altitude is shown in Figure 5.1.

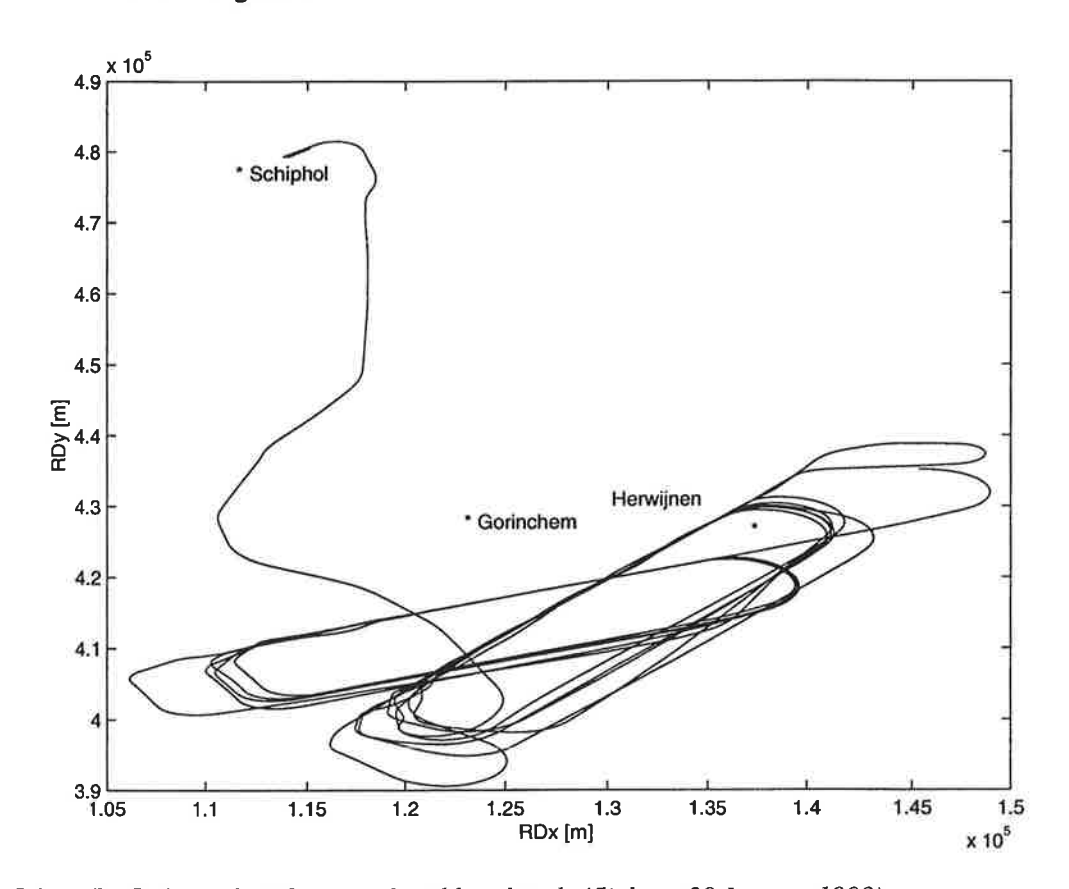


Figure 5.1: The flight track of the aircraft at 6 km altitude (flight on 29 January 1999).

The orbit starts at Schiphol, at the top in the figure. The two rectangular structures at the bottom correspond to the repeated 33 and 63 degree tracks. The radar looks to the left, to Gorinchem, so both rectangles were traversed clockwise (with one exception - see below). Consequently, the sides closest to Gorinchem are where the radar was active. The slant distance to the reference station near Herwijnen was about 22 km at the start of the track, 6 km minimum (when the aircraft flew over the reference station), and 40 km at most.

Analysis of the GPS data was carried out using various procedures:

- Analysis of the raw data on cycle slips and multipath effects using the monitoring software, developed at the Sub-faculty of Geodesy of TU Delft [de Jong and Jonkman, 1999]. Conclusion: the raw data collected in the aircraft has very few cycle slips and multipath errors.
- Analysis of the internal precision (among others the residuals after adjustment) using GPSurvey.
 Conclusion: the RMS value for the position is generally less than 2 cm, per satellite it is less than 5 cm.
- Analysis of the differences between code (DGPS) and carrier phase positions processed with GPSurvey [van den Heuvel and Husti, 1998]. Conclusion: the differences are generally less than 1 m in the horizontal position and less than 2 m in the vertical position.
- Analysis of the differences between the positions processed with GPSurvey and GeoGenius [Husti, 1999]. Conclusion: the differences in the horizontal positions are a few centimetres, in the vertical positions an offset of 12 cm was detected, which should be further investigated.
- Analysis of the differences between the aircraft positions obtained with the two reference stations
 Delft and Herwijnen, processed with GPSurvey. Conclusion: the differences are only a few
 centimetres.
- Processing the static baseline Delft-Herwijnen (52 km) with GPSurvey and comparison of the thus derived position of Herwijnen with known WGS-84 co-ordinates, [van den Heuvel and Husti, 1998; Husti, 1999]. Conclusion: the mean deviation in the horizontal position is 1 cm (maximum value 2 cm) and in the vertical position 4 cm (maximum value 8 cm).
- Analysis of the GPS positions processed with the "IT" software [Joosten, 1999]. Conclusion: this software is more suitable for long ranges and not so much for this project.

5.2 Horizontal distance between planned and flown tracks

With this data above it was easy to extract those parts of the total track flown close enough to the planned tracks (Table 4.3). The horizontal distances to the planned tracks are plotted in Figure 5.2.

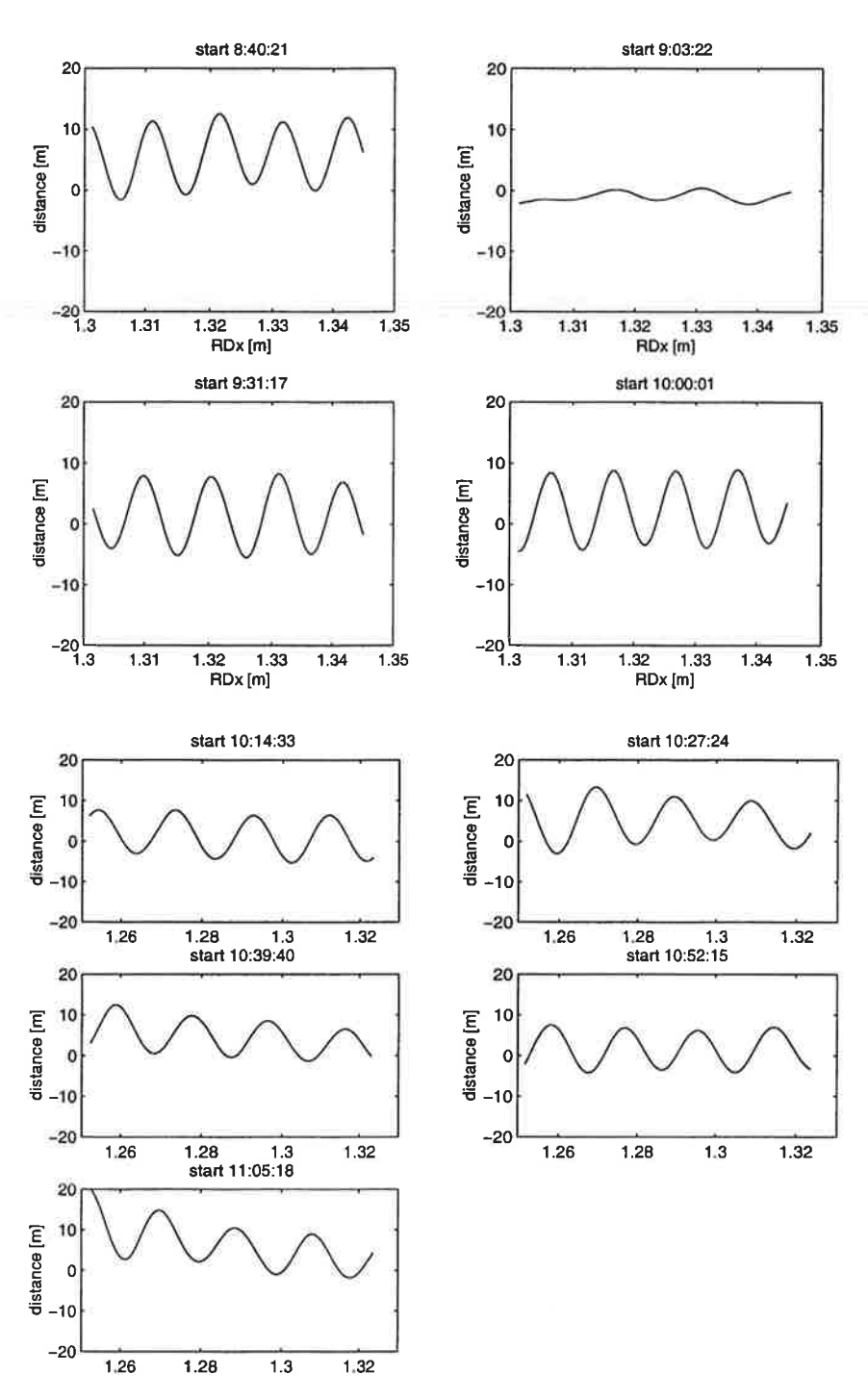


Figure 5.2: Horizontal distances from 33 degree (top) and 63 degree (bottom) planned tracks to the tracks flown. The plots cover the 8 km planned. The horizontal distance is plotted as a function of $RDx/10^5$ m, not the distance along the track.

The following is clear:

- 1. the horizontal distance is below about 10 m in almost all cases
- 2. all tracks oscillate, with about 4 periods in the 8 km track (one period takes ≈24 seconds due to the ≈85 m/s flight speed). The amplitude is 7 m on average, except in one case (see next point).

- The oscillation is thought to be the natural frequency of the aircraft-auto pilot-DGPS system explained in section 3.2.1.
- 3. the track starting at 9:03:22 is (a factor five) smoother than the others. That track was flown (for testing purposes) in the opposite direction (making it impossible to acquire radar data of Gorinchem), with tail wind. Why this results in a smaller oscillation is not clear yet⁶.

The oscillation of point 2 can be approximated by

$$d = 7\sin\left(\frac{2\pi}{2000}x\right),\tag{5.1}$$

with d the cross track distance [m] and x the along track distance [m]. The track direction is given by

$$\alpha = \arctan(d') = \arctan\left(\frac{14\pi}{2000}\cos\left(\frac{2\pi}{2000}x\right)\right),\tag{5.2}$$

which varies between $\pm 1.3^{\circ}$. So although the orbit's position is (in the horizontal plane) almost always well within the 10 m limit of section 3.1.2, the beam azimuth angle varies within $\pm 1.3^{\circ}$ (if the antenna beam direction would be fixed with respect to the orbit direction), instead of the $\pm 0.3^{\circ}$ required.

5.3 Line of sight (LOS) and depression angle analysis

The next step in the orbit analysis was the computation of line of sight and depression angles (Figure 5.3). For this computation we had to use both orbit and attitude data.

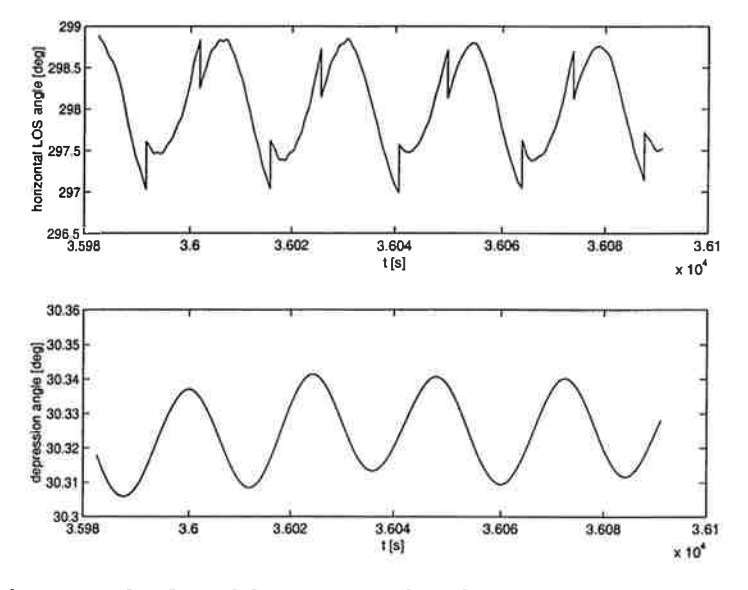


Figure 5.3: Line of sight and depression angles of run 5, plotted as a function of time.

⁶ The "begin" and "end" of the landing strip were exchanged when loading them into the auto pilot. However, this cannot be the cause of the oscillation, according to the NLR.

The line of sight (LOS) angle is defined in appendix C: the angle between the north and (the main direction of) the beam, projected onto the horizontal plane. It is computed with Eq.(C.2). The depression angle is the angle between the horizontal, and the line (in the LOS direction) connecting the antenna and a point on the ground (which in turn is located on a straight line parallel to the average flight track, at exactly 12 km slant range for the first point of the track). We observed the following:

- 1. the sudden jumps in the LOS angle are due to the beam steering (run 5 used the geographical beam steering mode). Although the beam is steered in the right direction (i.e., decreasing the LOS variation), this is not done frequently enough. This also causes an offset (from the expected average value of 270+33=303°). It turned out that this was due to an error in the on board beam steering software⁷. Without this error the LOS angle differs no more than a few tenths of a degree from 303° (simulation result).
- 2. the depression angle varies within 0.04°. The average is slightly higher than 30° because of the altitude exceeding the 6000 m planned.

Inspection of similar plots for all runs led to Table 5.1.

Table 5.1: Depression and LOS angle intervals. The number between brackets is the size of the interval.

run	depression angle [deg]	LOS angle [deg]
1	30.30 - 30.35 (0.05)	297.0 - 299.1 (2.1)
3	30.28 - 30.33 (0.05)	297.0 - 299.0 (2.0)
5	30.31 - 30.34 (0.03)	297.0 - 298.9 (1.9)
6	30.33 -30.37 (0.04)	323.7 - 325.5 (1.8)
7	30.37 - 30.41 (0.04)	323.8 - 327.0 (3.2)
8	30.35 - 30.38 (0.03)	323.8 - 326.5 (2.7)
9	30.39 - 30.42 (0.03)	324.5 - 326.8 (2.3)
10	30.32 - 30.40 (0.08)	324.2 - 326.3 (2.1)

The depression angle of all runs is between 30.28° and 30.42° . This implies that the worst (largest) perpendicular baseline is $12000 \times (30.42-30.28) \times \pi/180 \approx 29$ m. In all other cases the baseline is well below the 20 m limit of section 3.1.2. As a consequence, range spectrum filtering will only marginally improve the coherence, and is therefore not needed.

The situation is entirely different in azimuth. Even within a run the LOS angle varies up to 3.2° (run 7), due to the oscillatory nature of the orbit (Figure 5.2). Whether and when the LOS difference between runs is below the 0.6° limit of section 3.1.2 depends on the relative phase of the orbit oscillations. This is shown below. Note that the LOS interval of the geographical steering runs (5, 7 and 10) is not smaller than those of the other runs, due to the failing steering program.

The LOS angle difference of all possible combinations of runs (within the groups 1,3,5 and 6,7,8,9,10, of course) is shown in Figure 5.4.

⁷ This error also stopped steering during the active beam steering mode. The beam direction was erroneously kept constant throughout in that mode.

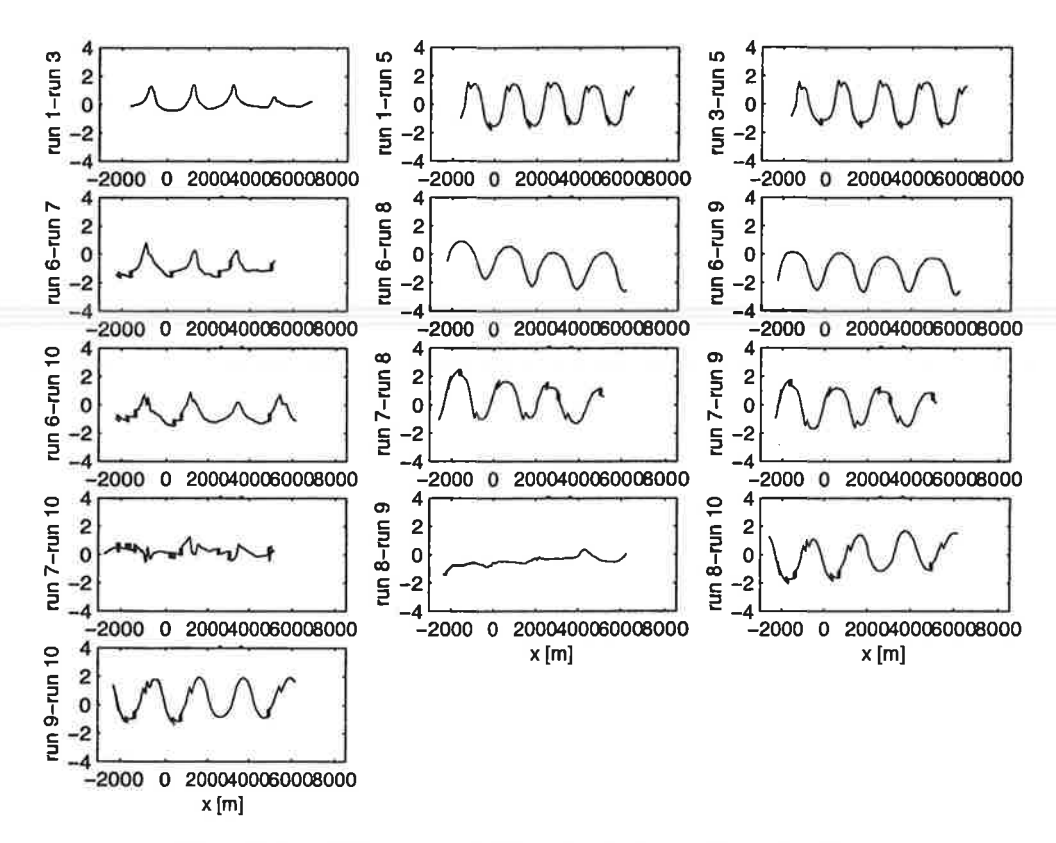


Figure 5.4: Difference in LOS angle of all possible pairs of runs.

Almost all LOS difference curves oscillate heavily. The best pairs (smallest LOS angle difference) seem to be runs 7-10, 1-3 and 8-9.

5.4 SAR data

The GSP (Generic SAR Procesor) normally used for PHARUS data was modified for RPI processing as follows:

- 1. a user defined reference track (an imaginary straight flight track, used during processing) was implemented. This enables one to process the slave data with a track parallel to that of the master. This leads to straight flat earth fringes.
- 2. the pixelsize was rounded to the nearest 2 cm multiple. This is necessary for interferogram generation: the master and slave should have the same pixel size.

Also some RPI GSP processing parameters were different from the ones used normally. For example, the azimuth reference function was updated every pixel, instead of every block of 10 pixels. In this way phase jumps are prevented (at the expense of a longer processing time).

Figure 5.5 shows the SAR image of run 10. Gorinchem is partially visible at the lower right, above the river Merwede.



Figure 5.5: Image of run 10 (near range at the bottom; dimensions: 6338 m azimuth×5778 m slant range).

The lower right part corresponds to the topographic map of Figure 4.1.

Several images showed the following phenomena:

- broad dark light bands oriented almost vertically. These are caused by the oscillating LOS angle (section 5.3), which is in addition offset from the required value. This causes the spectrum to shift periodically outside the Doppler window sampled (Table 4.4: window width= PRF/presum factor= 1000 Hz). This results in a loss of recorded power, and thus brightness in the image. The number of dark bands is equal to the number of LOS oscillations: one per 2 kilometre.
- short, light lines, perpendicular to the bands. No point target is visible which causes these lines (side lobes?). Because the lines are found at the same position in images with identical track angles, the cause has to be ground bound (possibly outside the image).

Figure 5.6 shows the (bright) response of the eight corner reflectors (4 at the top, 2×2 at the left) installed at the dike, our target of interest.

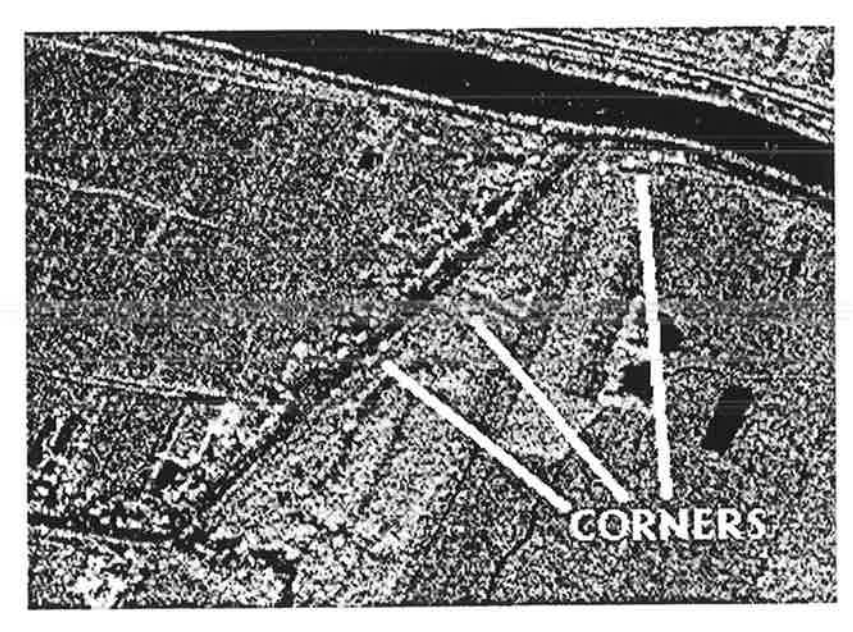


Figure 5.6: Corner reflectors.

The corner reflector signatures were used to verify the image resolution, which is expected to be about 1 meter in azimuth and 3.4 m in range⁸. The range resolution turned out to be right, but the azimuth resolution was as bad as 50 m in some cases, and as bad as 2-5 m in the other cases. Because increasing resolution leads to decreasing coherence (section 3.1) considerable time was spent on improving the azimuth resolution. After improving the way in which the IRS and GPS data were combined (section 3.3.2) we achieved satisfactory resolutions⁹. For 4 corner reflectors in the run 7 and 10 images the azimuth resolution is within the 0.92-1.24 m range, and the range resolution within 4.55-5.24 m.

⁸ Actually, a known shortcoming of the SAR processor with respect to range migration handling causes this value to degrade to about 5 m.

⁹ We also corrected a wavelength error in the GSP (we used erroneously the former PHARS wavelength of 5.7 cm instead of the 5.66 cm of PHARUS), which possibly also caused some improvement.

6. Interferometric data analysis I

6.1 Interferograms

6.1.1 Run 7 and 10: 2.5-2.9 m azimuth resolution

One of the first things done was the computation of an interferogram of a part of run 7 and 10 (one of the promising couples according to Figure 5.4). This was done before the azimuth resolution spoiling errors of the previous section were discovered: the azimuth resolutions were on average 2.5 m for run 7 and 2.9 m for run 10. The pixel size was 0.32 m in azimuth and 3 m in slant range. The algorithm for interferogram generation was:

- extract equally sized rectangular patches (including the dike and corner reflectors; 20000 azimuth×240 range pixels) from the images, with complex pixels.
- shift the images such that one of the corner reflectors appears at the same position in the images (coarse, pixel level co-registration). This assumes perfect geometric fidelity of the images.
- compute the complex coherence ρ for non-overlapping patches of 25 azimuth pixels×3 range pixels with:

$$\rho = \frac{\sum_{i=1}^{75} s_{7,i} s_{10,i}^*}{\sqrt{\left(\sum_{i=1}^{75} \left|s_{7,i}\right|^2\right) \left(\sum_{i=1}^{75} \left|s_{10,i}\right|^2\right)}}$$
(6.3)

with $s_{7,i}$ ($s_{10,i}$) a complex pixel of the run 7 (10) image. This provides the interferogram as a 800 azimuth×80 range pixels image (8 m×9 m pixel size), of which the amplitude and phase are shown in Figure 6.1. The amplitude image is shown at the top for reference.

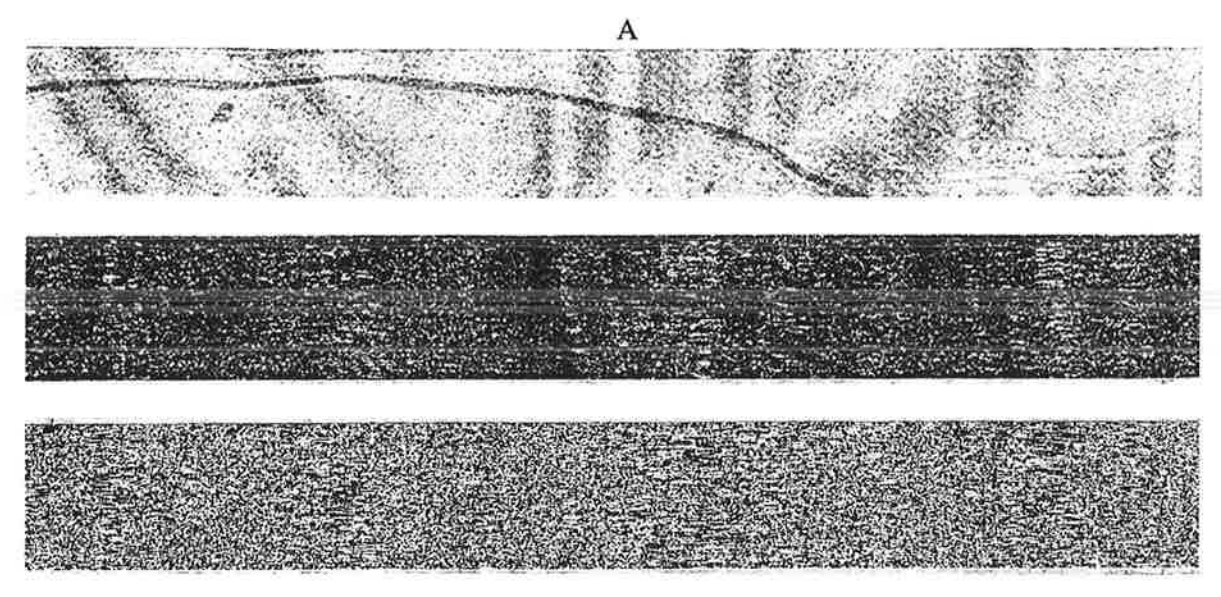


Figure 6.1: Top: amplitude image (the more or less vertical bands are scanner/printer artefacts). Middle: absolute value of the coherence. Bottom: phase of the coherence.

The most prominent feature in the amplitude image is the Kanaal van Steenenhoek, extending from the upper left to (almost) the lower right. The dike is barely visible underneath marker A, below the Kanaal. The absolute coherence image features dark vertical bands. This coherence loss is most probably due to the large azimuthal beam direction difference, varying along the way. The Kanaal shows up dark, especially underneath marker A (compare amplitude image). The Kanaal's coherence is about 0.13, the brighter parts surrounding it exhibit an average coherence of 0.24. So there seems to be at least some coherence present. Underneath the bright (high coherence) bands (in the middle figure) the phase seems to correlate in the coherence phase image (the bottom figure), as is to be expected.

The coherence is expected to increase if we:

- process the images to the correct azimuth resolution of about 1 m.
- shift every 25×3 pixel patch of run 10 relatively to that of run 7, in order to find the highest coherence. This largely circumvents the geometric fidelity criterion.

The next section describes the results of these improvements.

6.1.2 Run 7 and 10: 1.2-1.4 m azimuth resolution

Run 7 and 10 were re-processed to a better azimuth resolution than above: on average 1.4 m for run 7 and 1.2 m for run 10 (apparently run 7 is still not processed optimally). After inclusion of the shift operation mentioned above we got the results of Figure 6.2, which is in the same format as Figure 6.1. It should be noted that the interferogram area is smaller than that of Figure 6.1. Marker A again indicates the dike.

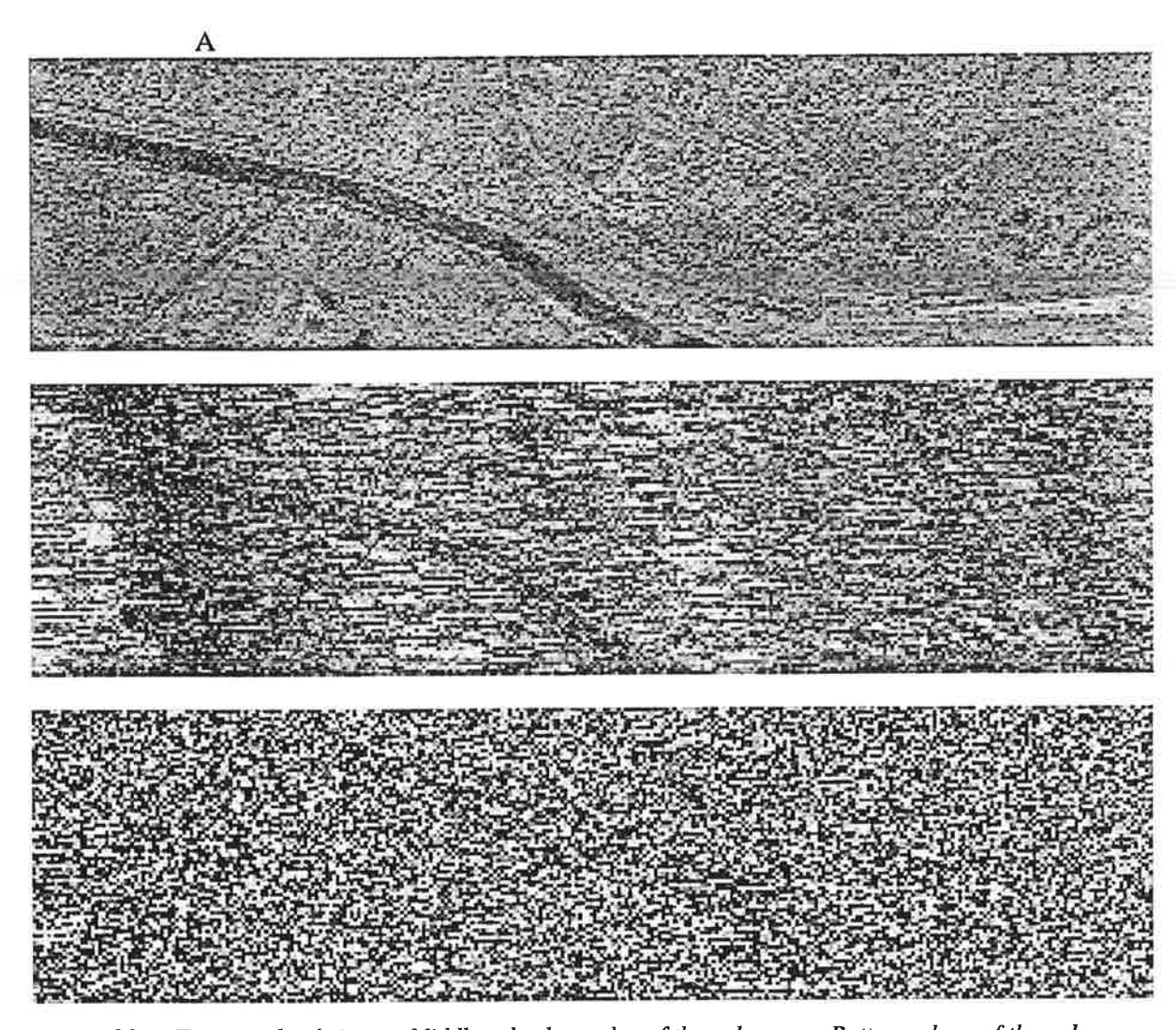


Figure 6.2: Top: amplitude image. Middle: absolute value of the coherence. Bottom: phase of the coherence.

The contrast between high and low coherence areas is much higher now: on average 0.83 for the bright areas (land), and 0.48 for the water areas. This relatively large value of 0.48 is due to the shift operation. However, in this case there is no indication of a correlating phase at the high coherence positions. This suggests that the shifting operation selects the largest coherence, but not necessarily the shift providing optimal phase correlation. This is also confirmed by the random character of the shift, which is expected to be slowly varying over the image. Therefore we processed the same images, but now without the shift operation (Figure 6.3).

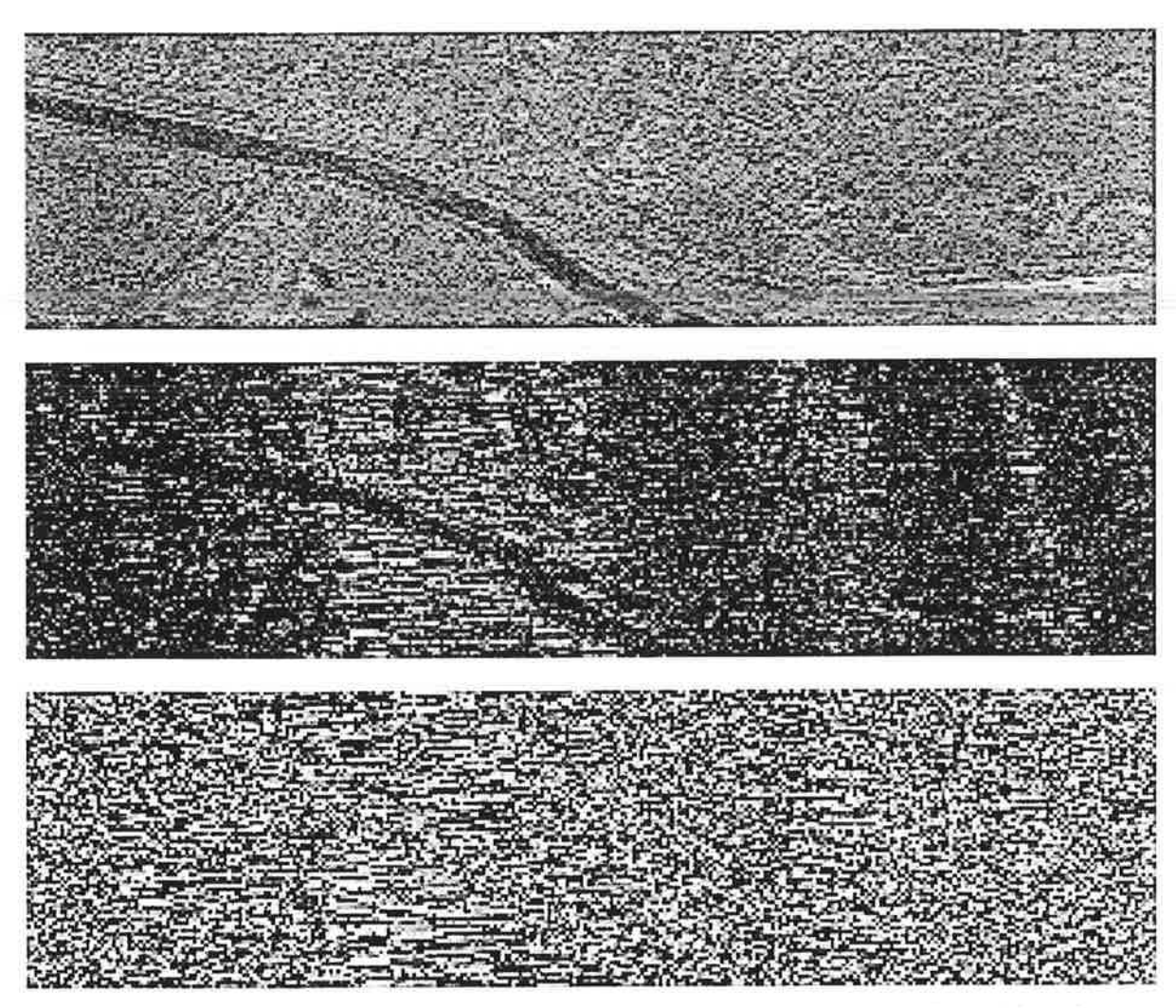


Figure 6.3: Top: amplitude image. Middle: absolute value of the coherence. Bottom: phase of the coherence.

In this case the bright area coherence is 0.41 and the dark area coherence 0.15, a clear improvement compared to Figure 6.1. The increase of 0.24 (2-3.5 m azimuth resolution) to 0.41 (a factor 0.41/0.24=1.7) corresponds roughly to the resolution improvement (an average factor of 2.7/1.3=2.1), as expected from Eq.(3.3).

6.2 Spectral analysis

Coherence loss due to azimuthal beam direction differences can be easily quantified by computing azimuthal spectra of the master and slave images [Geudtner, 1995]. If the position differs too much the overlap between the spectra is lost and so is the coherence. Simply put, a reduced coherence ρ' results from a real (underlying) coherence ρ , according to

$$\rho' = \left(1 - \frac{\left|f_{DC,1} - f_{DC,2}\right|}{W}\right) \rho \text{ if } \left|f_{DC,1} - f_{DC,2}\right| < W, \text{ 0 otherwise.}$$
 (6.4)

 $f_{DC,I}$ and $f_{DC,I}$ are the Doppler centroids of the two spectra, and W the (identical) widths, all in Hz. For PHARUS $W\approx284$ Hz, as computed from the spectra. Figure 6.4 shows the results of a spectral analysis.

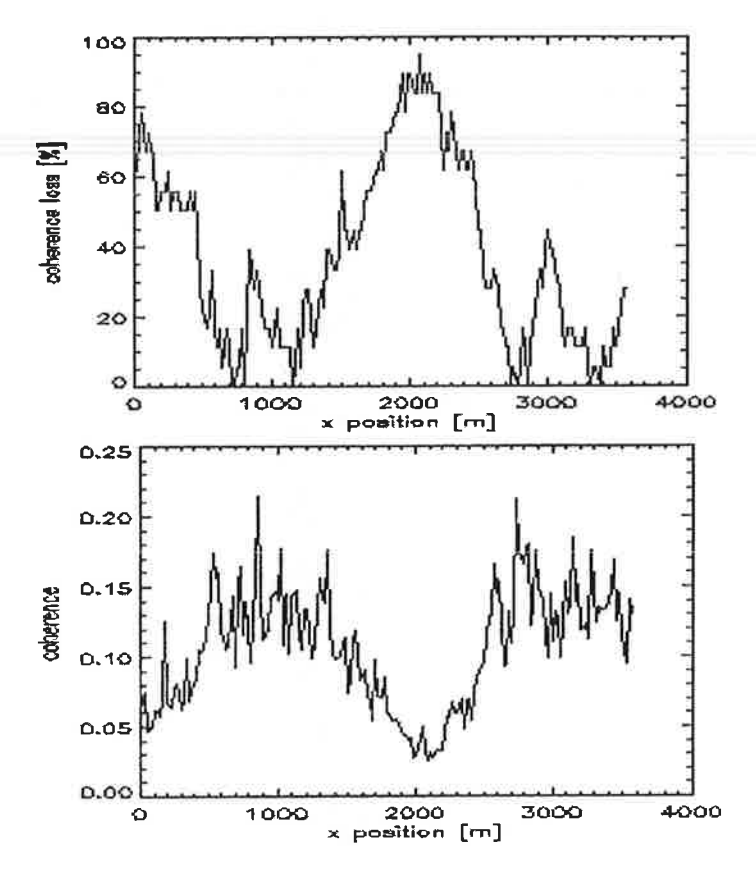


Figure 6.4: Expected coherence loss (top) and actual coherence (bottom) as a function of azimuth position x. The algorithm used is:

- extract equally sized rectangular patches (9000 azimuth×32 range pixels, corresponding to 2880 m azimuth×96 m slant range) from the images. The images are already co-registered by using one corner reflector as a tie point.
- compute the spectra over blocks using 64 azimuth×32 range pixels, by averaging 32 azimuth spectra computed over 64 pixels.
- find the Doppler centroids of the two spectra., $f_{DC,1}$ and $f_{DC,2}$.
- compute the expected coherence loss $100 \times |f_{DC,I}-f_{DC,2}|/W$ [%] (top of Figure 6.4)
- compute the maximum actual coherence (by eventually shifting one patch with respect to the other) of every 64 azimuth×32 range pixel patch (bottom of Figure 6.4).

As expected, the coherence drops if the spectral overlap diminishes 10 . Nevertheless, the coherence is small: even if the spectral overlap is 100 % (coherence loss= 0%), as is the case at $x\approx2900$ m, the coherence is only 0.2.

¹⁰ In another case analysed this relation is less clear.

6.3 Additional findings

The yaw of the aircraft was typically -16 degrees. The incorrect beam steering was not able to compensate sufficiently for this large value. The compensation (the planned track angle minus the horizontal LOS angle) was only some 6-10 degrees, leaving -6 to -10 degrees of uncompensated yaw. This uncompensated yaw is the angle between the zero Doppler direction (the direction perpendicular to the instantaneous flight direction) and the antenna beam direction. It leads to corner reflector responses which do not match across image patches processed with separate azimuth reference functions (Figure 6.5).



Figure 6.5: Fragmented corner reflector responses.

The top (A' and B') of the reflector responses is shifted to the left with respect to the bottom (A and B). It is clear that this phenomenon hampers correct co-registration. If the azimuth reference function is updated every azimuth line the fragmentation changes to its smooth equivalent: the responses become squinted themselves, which is also not desirable. Correct beam steering would largely eliminate this problem.

The above phenomenon is also illustrated by the following: about 10 corresponding point target response pairs (e.g., pairs corresponding to the same corner reflector) were selected in two master/slave pairs. The images of the first pair were processed with the azimuth reference function updated every 10 azimuth lines, those of the second updated every azimuth line. Assuming that the first point pair coincided (i.e., one-point co-registration) we observed the shifts of Table 6.1.

Table 0.1.	Kunge unu uzii	
	10 line update	1 line update
range shift [m]	3 to 6	-3 to 0
azimuth shift [m]	-19.2 to -5.8	-1.6 to 2.6

Table 6.1: Range and azimuth shifts.

The range shift interval is small enough with respect to the 5 m range resolution. This is not the case for the azimuth shift interval compared to the azimuth resolution of some 1.1 m. It is clear that more frequently updating the azimuth reference function improves the geometric fidelity of the images. Nevertheless, the remaining spread (due to inaccurate orbit data?) of -1.6 to 2.6 m is insufficient. For interferometric purposes it can be corrected for by computing an interferogram from small corregistered patches.

7. Interferometric data analysis II

Because the analysis of the data (of 29 January 1999) in the previous chapter did not lead to good interferograms, we decided to incorporate in this report an extended analysis of data acquired on 3 February 2000¹¹. For this analysis more effort was put in adaptation of the GSP and the interferometric software. Because the radar data characteristics are similar to those of January 1999, these are not discussed¹². Instead, this chapter describes the software changes briefly and presents results of the improved processing.

7.1 GSP changes

In order to improve the quality of the interferograms we implemented the following changes in the GSP:

- 1. The master and slave are processed with an identical reference track (i.e, having the same starting point and direction), instead of with parallel reference tracks only, as before. This prevents occurrence of fringes parallel to the flight tracks.
- 2. From a comparison of beam switching moments in the radar data (which are visible as Doppler centroid ¹³ jumps) and the corresponding times reported in the data headers it appeared that switching occurred 0.5±0.05 seconds earlier than reported. Therefore a 0.5 second time shift (to earlier times) was applied to the beam data.
- 3. The time increment of the motion datafiles is not a constant 0.02 seconds, as expected. Therefore the time increment is set to the constant (end time-start time)/(number of lines-1).
- 4. A cosine phase correction is applied in the azimuth correlator, which compensates for the beam direction not being perpendicular to the reference track
- 5. Processing block dimensions in azimuth are not rounded to a multiple of eight in the azimuth correlator. This eliminates phase jumps in the interferogram.
- 6. The pitch, yaw and beam angles of the master and slave flight data are averaged. During computation of the centroid direction by the azimuth correlator the LOS velocity term is put to zero. The direction depends therefore on the pitch, yaw and beam only. Because these are identical for the master and slave (due to the averaging above), the centroid is also the same. The net effect is that block borders are invisible in the interferogram, because they coincide for the master and slave images.
- 7. The averaged angles are low pass filtered (without introducing a delay) to eliminate fast interferometric phase changes.
- 8. The left azimuth margin is taken equal for the master and slave, which causes both images to start at the same point on the ground. This aligns even more block boundaries.

¹¹ These data were acquired within the framework of the BCRS project "2-D Deformation with ASAR/PHARUS" (2.3/AP-03).

¹² It should be noted that the error in the beam steering software (section 5.3) was corrected before this data was recorded

¹³ The Doppler centroid was computed with the sign-Doppler algorithm from [Madsen, 1989].

7.2 Results

After applying only step 1 the master and slave image were combined into an interferogram with the freely available Doris software package [Kampes, 1999]. This program is intended to be used for ERS data, but can be adapted for airborne data. The coherence of land was up to 0.65, of water 0.11 (150 looks). The most important finding was the occurrence of discontinuities in the co-registration, indicating that the master image is at some positions suddenly stretched in azimuth with respect to the slave. Shifts of up to 5 m occur. This implies that the PHARUS images are not geometrically correct down to meter level. This could be due to the orbit used, or to the GSP.

Next we produced an interferogram ourselves. The relative deformation of the master and slave is up to 5 meters. In addition, one image was defocused (i.e., it had an average azimuth resolution of 1.7 instead of 1.0 meters). Both can be caused by wrong motion data. We employed an autofocus routine on the defocused image. This routine provides orbit corrections, which should lead to a well focused image. Although the focus was indeed restored, the required orbit changes were up to 5 meters. Because the motion data exhibit about 20 cm vertical accuracy and 10 cm lateral accuracy, these are unrealistically large changes. If the motion data is correct, possibly the GSP is responsible for the incorrect geometry.

We created an interferogram of a selection of the complete image with the highest coherence. The amplitude, coherence and phase are shown in Figure 7.1. A dike (extending from image coordinates (2500,110) to (5000,40)) is visible in all three images. It is possible to estimate its height relative to its surroundings by measuring the relative phase. The phase difference turns out to be 0.79±0.06 radians. The phase difference due to a height difference is

$$\Delta \phi_{topography} = \frac{4\pi B_{\perp}}{\lambda H \tan \theta} \Delta h_{topography} \tag{7.1}$$

with

 $\Delta \phi_{topography}$ phase difference due to topography [0.79±0.06 rad] perpendicular baseline [5 m]

 λ perpendicular baseline [5 if λ wavelength [0.0566 m] H flying height [6006 m] θ look angle [57 deg]

 $\Delta h_{topography}$ topographic height difference [m]

This leads to a height estimate of 6.6±0.5 m. From [Wolters-Noordhoff Atlasprodukties, 1987] the dike height is between 5.8 and 6.2 m (relative to its surroundings), close to our measured value. The most uncertain factor (not included in the 0.5 m error estimate) in this calculation is the baseline. Thus it is likely that once all artefacts are removed from the interferogram quantitatively correct information can be derived from it.

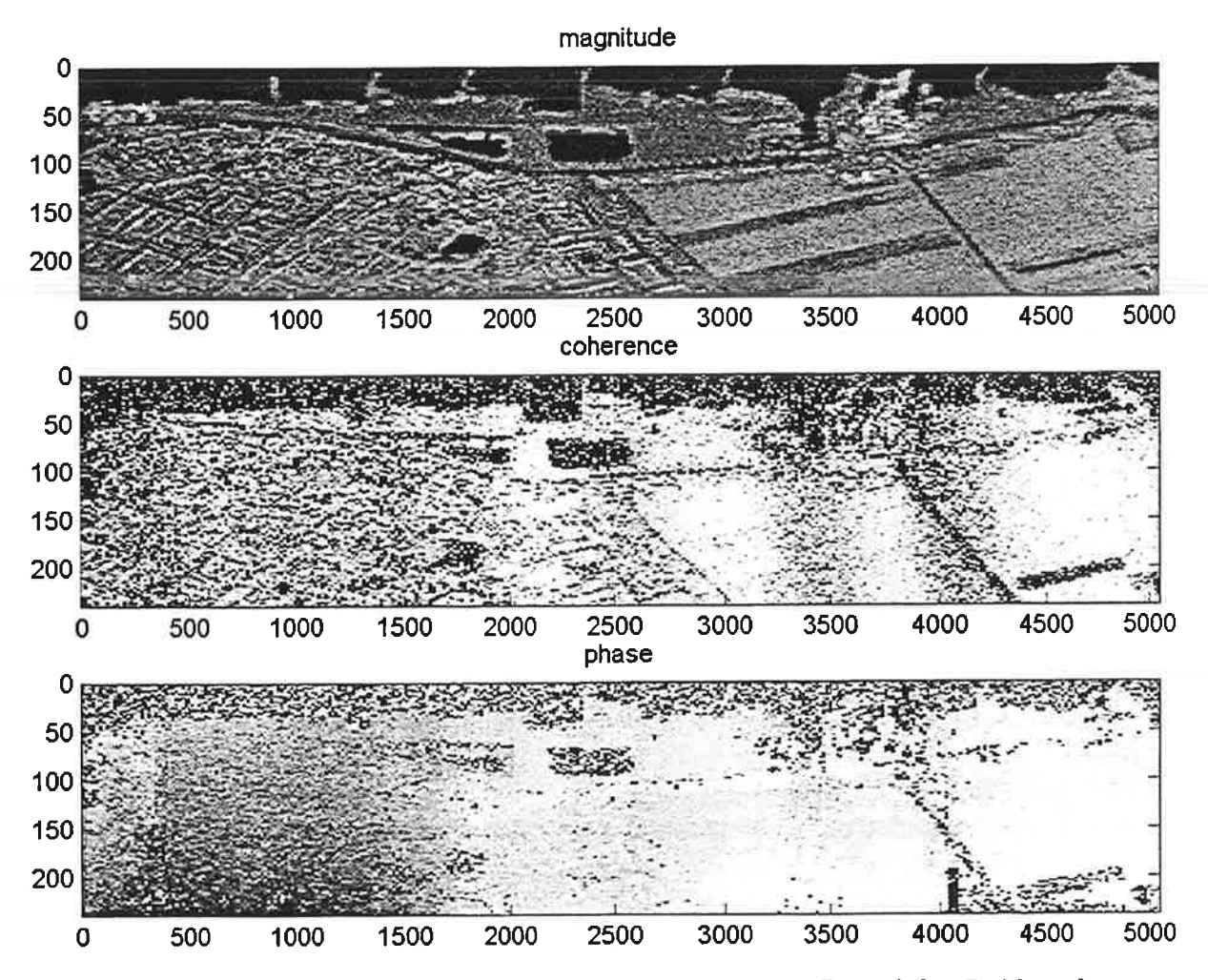


Figure 7.1: Magnitude, coherence and unwrapped phase of a small area below De Merwede.

8. Conclusions and recommendations

8.1 User requirements

8.1.1 Conclusions

Measuring deformations of dikes by means of an airborne interferometry SAR technique using PHARUS can be very useful, though it has to meet a few strict demands:

- The system has to be sufficiently available for use for the safety assessment every five years and for regular monitoring purposes and the results must come available in a suitable format.
- During the high water season the system has to be available at a few days notice and the results have to come available in a suitable format within 4 to 8 hours.
- The system should be able to measure settlements deformations of 1-3 cm with 1 cm accuracy.

If sufficient water boards and other water defence managers in the Netherlands can use this system for regular water defence management, the five-yearly safety assessment and high water management, it can be profitable to exploit this system for the aforementioned purposes.

Since the system could also be useful for road maintenance and management one questionnaire was send to an advisor for road design and maintenance. The response was very positive.

8.1.2 Recommendations

The possibilities, properties and price of the airborne interferometry SAR technique using PHARUS have to be evaluated in detail for the water defence managers in The Netherlands. Next a thorough feasibility study has to be executed including representatives from the water defence managers so as to determine legal, administrative, and logistic matters

The price of the system is probably rather high. Therefore it is necessary to execute a thorough 'market research' before the system is further developed for use for water defence management.

It is also recommended to investigate the possibilities for road management further.

These aspects are already largely covered in the BCRS project '2-D deformation with ASAR/PHARUS' (BCRS 2.3/AP-03) by the consortium carrying out the here presented project.

8.2 Continuous kinematic GPS by postprocessing using phase measurements

8.2.1 Conclusions

8.2.1.1 Measurements

- Continuous kinematic GPS tracking in an aircraft does in general not give many problems. The data contains very few cycle slips and is hardly affected by multipath. To avoid cycle slips it is recommended that the pitch and roll of the aircraft during the flight are below 15°.
- The measurements require a sufficient number of satellites (≥ 5) and a good geometry (PDOP < 6) for an elevation mask of 15°.

8.2.1.2 Postprocessing

- Using carrier phase observables it is possible to obtain positioning results at levels <10 cm.
- Several software packages are available for postprocessing. However, there are many considerable differences between the software packages GPSurvey, GeoGenius and Flykin that were compared for this project. The positions computed by GPSurvey and GeoGenius agree to within a few centimetres. The results obtained with Flykin are not satisfactory.
- Resolving the carrier ambiguities over larger distances (> 20 km) remains a problem. GPSurvey supplies the most reliable positions, even over larger distances.
- Quality control and quality indicators are very essential.
- Data analyses on cycle slips, multipath and other errors are desirable. The monitoring software developed at the Delft University of Technology appeared to be very useful.

8.2.2 Recommendations

8.2.2.1 Measurements

- It is necessary to use geodetic dual-frequency (L1 and L2) receivers (like the Trimble 4000 SSi) and compatible antennas, i.e., antennas dedicated to the receivers being used.
- It is recommended to set up at least two ground-based reference stations in order to be able to cross-check the results. The WGS-84 co-ordinates of the reference stations must be known to within 1-2 cm.

8.2.2.2 Postprocessing

• The software package Flykin should be improved to become useful in a production-type of environment ¹⁴.

¹⁴ Flykin was only tested in this project, and not used to compute the orbits input to the SAR processor.

8.3 Data analysis

8.3.1 Conclusions

- Levelling revealed 6 cm subsidence between September 1998 and January 1999 of our object of investigation, the dike near Gorinchem.
- The aircraft orbit was almost always within 10 m from the planned track (in the horizontal plane).
- The aircraft orbit oscillates in such a way that the horizontal LOS angle varies too much for interferometric purposes.
- This oscillation was not compensated for by the (geographical) beam steering mode, because the beam steering did not function properly.
- The oscillation did not influence the depression angle (at a fixed point on the ground) significantly.
- The dm-accuracy Trimble GPS orbit data proved to be of great use for quick selection of the data suitable for interferometry.
- The correct integration of Trimble GPS and IRS data proved to be critical for achieving 1 m azimuth resolution in the SAR images.
- Because of the large azimuthal beam offset due to the incorrect beam steering the SAR images exhibit geometrical errors, which are related to interferometric phase errors.
- It was possible to compute an interferogram of a relatively error free part of the master and slave. The dike height estimated from the phase differs only a few decimetres from the topographic map value.
- Although a lot has been learnt from the current project concerning airborne repeat pass interferometry, it was not (yet) possible to measure the deformation of the Wolpherense Dijk. Better results are expected in the near future.

8.3.2 Recommendations

- The aircraft's orbit oscillation should be damped by modifying the real time orbit control.
- The beam steering should be implemented correctly 15.
- By taking the GPS and IRS characteristics into account the orbit resulting from Trimble GPS/IRS
 data integration could possibly be improved. This is a known problem, of which the regular
 solution involves extensive Kalman filtering.
- Another method of obtaining a good orbit is to use a SAR with two antennas, separated across track (an across track interferometer). The data of these two antennas enables one to compute the orbit parameters relevant for repeat pass deformation measurements.
- If the problem of image distortions related to phase errors remains, a solution might be to simulate raw data (given a regular array of point targets and motion data) and compute the resulting scene with the GSP. If the image is undistorted, the motion data is probably incorrect (and the GSP correct), otherwise, the GSP is probably incorrect (and the motion data correct) (assuming a flawless simulation, and the GSP and motion data not both being wrong).

¹⁵ At the time of writing an error in the on board beam steering software had been found and corrected. The data of chapter 7 was acquired with correct beam steering.

9. References

Gatelli, F., Guarnieri, A.M., Parizzi, F., Pasquali, P., Prati, C., and Rocca, F., 1994, The wavenumber shift in SAR interferometry, IEEE Tr. on Geoscience and Remote Sensing, 32, 855-865

Geudtner, D., 1995, The interferometric processing of SAR data, ESA-TT1341

Gray, A.L., and Farris-Manning, P.L., 1993, Repeat-pass interferometry with airborne synthetic aperture radar, IEEE Tr. on Geoscience and Remote Sensing, 31, 180-191

Hofmann-Wellenhof, B., 1997, GPS Theory and Practice, Springer, 4th edition, 1997

Heuvel, F.A. van den, and Husti, G.J., 1998, Bepaling van de positie van het vliegtuig met GPS voor de luchtkartering, GPS Nieuwsbrief no.2, nov.1998

Husti, G.J., 1999, Kinematische GPS over grotere afstanden, GPS Nieuwsbrief no.1, mei 1999

Husti, G.J., and Sluiter, P.G., 1998, Processing of aircraft data with Semikin-Flykin software, Delft Geodetic Computer Centre, Internal report

Jong, C.D. de, 1998, Signaalsterkte en precisie van codewaarnemingen van Trimble ontvangers bij gebruik van verschillende typen antennes, GPS Nieuwsbrief no.2, nov.1998

Jong, C.D. de, and Jonkman, N.F., 1999, GPS/GLONAS integrity monitoring, GPS Nieuwsbrief no.1, mei 1999

Joosten, P., 1999, Processing vliegtuig data met "IT" software, GPS Nieuwsbrief no.1, mei 1999

B. Kampes, Doris - Delft object-oriented radar interferometric software - User's manual and technical documentation, TU Delft, DEOS, august 1999

Madsen, S.N., Estimating the Doppler centroid of SAR data, IEEE Tr. on AES, Vol. 25, No. 2, March 1989, pp. 134-140

Miyawaki, M., Nagata, H., Sugawara, M., Shinme, H., Murata, M., Nohmi, H., Shimada, M., Sakurai, T., Kobayashi, S., Fujii, N., Nomura, K., Kitani, H., 1998, Airborne repeat-pass INSAR system, Proc. IGARSS 1998, pp. 2677-2679

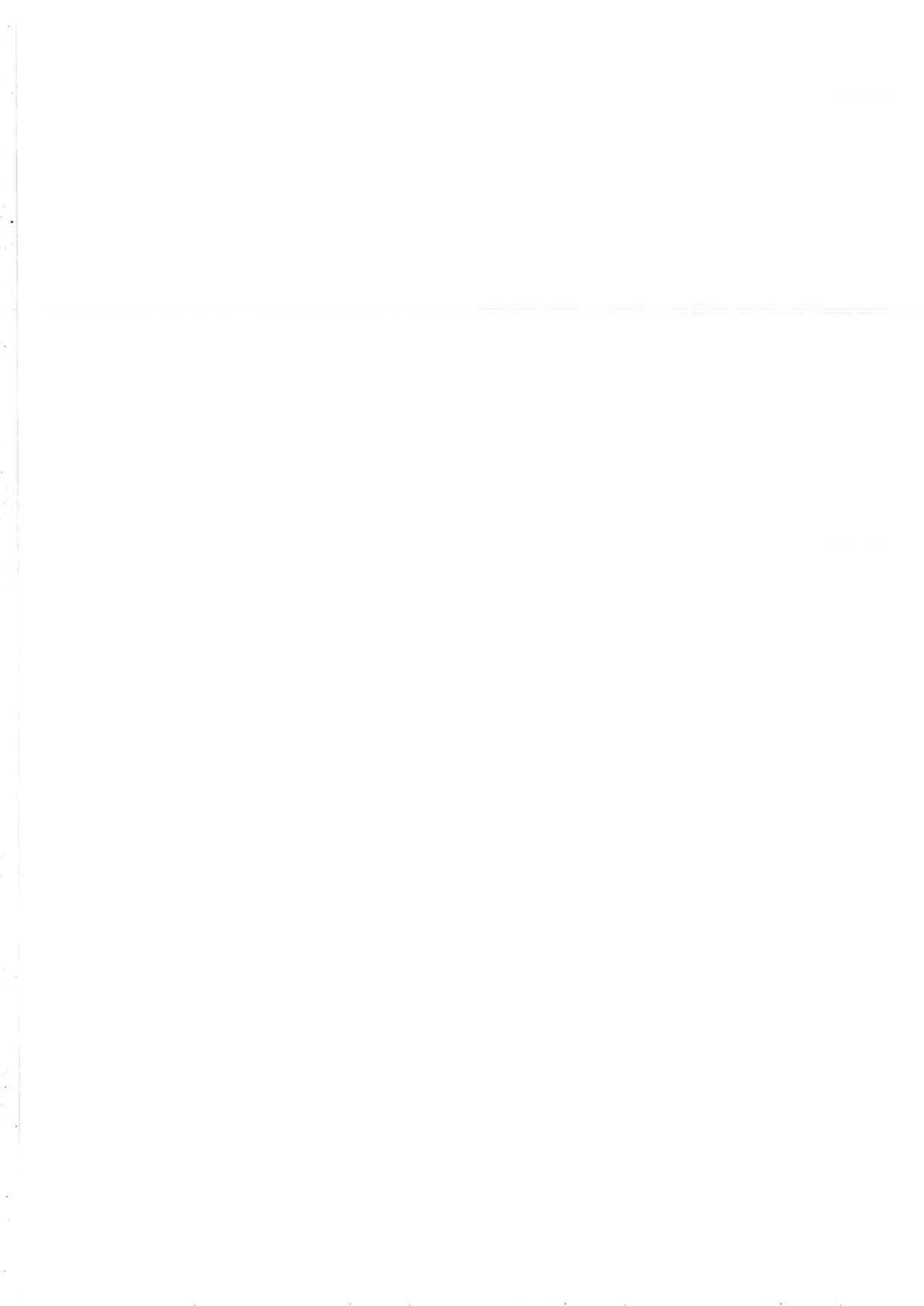
TAW (Technical Advisory Committee for Water Defences), 1994, Guideline for Safety Assessment ('Leidraad Toetsen op Veiligheid'), Road and Hydraulic Engineering Division (DWW), Delft

Teunissen, P.J.G., and Kleusberg, A., 1998, GPS for Geodesy, Springer – 2nd edition

Ulbricht, A., and Reigber, A., 1998, Airborne repeat-pass interferometry with DLR's experimental SAR (ESAR): first results, Proc. EUSAR 1998, pp. 241-244

Wolters-Noordhoff Atlasprodukties, 1987, Grote Topografische Atlas van Nederland, Wolters-Noordhoff

Zebker, H.A., and Villasenor, J., 1992, "Decorrelation in interferometric radar echoes", IEEE Tr. on Geoscience and Remote Sensing, 30(5), 950-959



Appendix A - Questionnaire (in Dutch)

Aan

Telefaxnummer

Van

P.J.L. Blommaart

Datum

18 mei 1999

Kenmerk

Doorkiesnummer

(015) 25 18 299

Telefoonnummer indien incompleet ontvangen

(015) 25 18 284

Aantal pagina's (inclusief voorblad)

10

Onderwerp

Ontwikkeling van een systeem voor de monitoring van zettingen en vervormingen van waterkeringen

Geachte,

Dijken en andere vormen van waterkering zijn niet volledig vorm- en plaatsvast. Onder invloed van het eigen gewicht en externe belastingen, zoals hoogwater, vervormt en/of verplaatst de waterkering enigszins. Deze vervormingen en/of verplaatsingen kunnen in extreme situaties tot falen van de waterkering leiden. Het is dan ook in het belang van de waterkeringbeheerder inzicht te hebben in het gedrag van de waterkering.

Dit inzicht kan algemeen of specifiek zijn:

- In het kader van een monitoring-programma ontstaat een algemeen inzicht in het vervormingsgedrag van de betreffende waterkering.
- In het kader van de vijfjaarlijkse veiligheidstoets dient inzicht te bestaan in de kruinhoogte en stabiliteit van de dijk.
- Tijdens hoogwaterperiodes dient inzicht te bestaan in de actuele situatie.

Om dit inzicht te verkrijgen zijn instrumenten en meetprogramma's nodig. Traditionele meetprogramma's maken gebruik van driehoeksmetingen en waterpassingen. Om een volledig inzicht te krijgen in de actuele situatie van de waterkering zijn deze methodes tijdrovend en daardoor duur. Onder auspiciën van de Beleids Commissie Remote Sensing wordt gewerkt aan een methode gebaseerd op interferometrische verwerking van gegevens van een onder een vliegtuig gemonteerde

radar. Met behulp van deze methode kan in korte tijd een inzicht in de actuele situatie van de waterkering verkregen worden over een grote strekking en niet uitsluitend in enkele vaste punten.

Het systeem wordt momenteel ontwikkeld om landdalingen en andere vervormingen over uitgestrekte gebieden te monitoren. Het systeem wordt ontwikkeld door TNO, het NLR en de TU Delft. GeoDelft, het Hoogheemraadschap van de Alblasserwaard en de Vijfheerenlanden en de Dienst Weg- en Waterbouwkunde van Rijkswaterstaat zijn betrokken bij het onderzoek naar de toepasbaarheid van het systeem voor waterkeringen.

Om inzicht te krijgen in wat nodig is om een zodanig systeem optimaal in te kunnen zetten voor het beheer van waterkeringen is het nodig inzicht te hebben in de wensen en behoeftes van waterkeringbeheerders. Om deze reden wil ik u verzoeken bijgevoegde vragenlijst te lezen en in te vullen en aan mij terug te faxen.

Bij deze telefax is enige algemene informatie 16 gevoegd omtrent de Beleids Commissie Remote Sensing, de lopende onderzoeksprogramma's en enkele projecten.

Bij voorbaat bedankt voor uw medewerking.

Met vriendelijke groet,

ir. P.J.L. Blommaart

Monmaart

Projectleider Geotechniek

¹⁶ Niet in dit rapport opgenomen.

Per vraag kunnen meerdere antwoorden mogelijk zijn.

1.	Wat moet een onder een vliegtuig gemonteerde radar waar kunnen nem □ verticale vervormingen (zettingen, kruinhoogte) □ horizontale vervormingen □ kwel	en?
	☐ wateroppervlakten achter de dijk	
	□ anders, nl.:	
2.	Met welke nauwkeurigheid moeten de waarnemingen uitgevoerd kunne	n worden?
	☐ verticale vervormingen (zettingen, kruinhoogte):	cm
	☐ horizontale vervormingen	cm
	☐ anders, nl.:	cm
3.	Met welke frequentie moeten metingen uitgevoerd worden?	
	uin het kader van de vijfjaarlijkse veiligheidstoets: uitsluitend de krui	nhoogte
	in het kader van de vijfjaarlijkse veiligheidstoets: zowel de vertical vervormingen	e als de horizontale
	☐ in het kader van monitoring:x per jaar	
	☐ tijdens een hoogwaterperiode:x per week	
	anders, nl:	
4.	Hoe snel moet een meting in geval van (aankomend) hoogwater uitgevo	oerd kunnen worden?
	☐ binnen 1 maand na aanvraag	
	☐ binnen 2 weken na aanvraag	
	☐ binnen 1 week na aanvraag	
	☐ binnen 3 dagen na aanvraag	
	☐ binnen 1 dag na aanvraag	
	anders, nl:	
5.	Hoe snel moet een meting in geval van de vijfjaarlijkse toets op de veili	gheid uitgevoerd kunnen
	worden?	
	binnen 1 jaar na aanvraag	
	□ binnen 6 maanden na aanvraag	
	binnen 3 maanden na aanvraag	
	□ binnen 1 maand na aanvraag	
	anders, nl:	

6.	Hoe snel moeten de gegevens in geval van hoogwater beschikbaar komen?
	☐ binnen 1 week na uitvoeren van de vlucht
	☐ binnen 3 dagen na uitvoeren van de vlucht
	☐ binnen 1 dag na uitvoeren van de vlucht
	☐ binnen 8 uur na uitvoeren van de vlucht
	☐ binnen 4 uur na uitvoeren van de vlucht
	anders, nl:
7.	Hoe snel moeten de gegevens in geval van de vijfjaarlijkse toets op de veiligheid beschikbaar komen?
	☐ binnen 3 maanden na uitvoeren van de vlucht
	□ binnen 1 maand na uitvoeren van de vlucht
	□ binnen 2 weken na uitvoeren van de vlucht
	□ binnen 1 week na uitvoeren van de vlucht
	anders, nl:
8.	In welke opmaak moeten de gegevens aangeleverd worden?
	☐ in platte tekst opmaak (ASCII)
	☐ in een spreadsheet-opmaak, namelijk:
	☐ in een tekenprogramma-opmaak, namelijk:
	☐ in een GIS-opmaak, namelijk:
	□ anders, nl:
€.	Zijn er nog onderwerpen, die niet in de voorgaande vragen aan de orde gekomen zijn, maar die wel aandacht behoeven? Zo ja, kunt u deze hier toelichten?

Appendix B - Responses to questionnaire (in Dutch)

Reacties op de vragenlijst ten behoeve van de ontwikkleing van een systeem voor de monitoring van zettingen en vervormingen van waterkeringen

HRS Alblasserwaard & Viffheerenlanden	ing E.J. Steenbergen	31 mei 1999	X	1 Cm	X	7x wk		aharikelijk van de beschlikbaanhekt, doch min een jaar na aanwraag
WS Vallei & EEM	P.G. Neienhile	28 mei 1969	X	10cm	X X	ahankelik van waarnemingen in hel. veld		**************************************
HRS Krimenpenerwaard	ing D an Schie	25 mei 1999		1 cm	X X]x wk		
HRS USHN	órs C Mass	Z1 mei 1999	X	< 5 cm < 5 cm < 5 cm b) een dreigende situalie: < 1 cm (zowel hor. als verl.)	X	2 à 3x / wk lydens dreigende situalies meerdere malen per dag	direct in geral van dreigende	X
DWW-IR	i AAM Vennens	19 mei 1999	X	1 cm T cm	i / A.	ingsbegeleiding Ingen)	nkvoeingespelekding.	monkaing
Respondent D organisatie	D rasan	O datum ontvangen	1 Wat most een onder een vlegtuig gemontearde radar waar Lunnen neman?	2 Met walte nauwkeuntgheid moelen de waannemingen uitgevoerd kunnen worden? U vertiske vervormingen G hotzoriale vervormingen D anders, ni	3 Met welte frequentle mosten matingen uitgevoerd worden? 0 in het kader van de vijfjaarlijkse veligheidstoels, uistuntend de kruinhoogle 0 in het kader van de vijfjaarlijkse veligheidstoels. Zowel de verticate als de horizontale vervormingen 0 in het kader van mondioning. It best kade	eek	4 Hoe snel moet een meting in geval van (aankomend) hoogwater uitgevoerd kunnen worden? U brinen 1 meaard na aanvraag U brinen 2 weken na aanvraag U brinen 1 dagen na aanvraag U brinen 3 dagen na aanvraag U brinen 1 dag na aanvraag U anders, ni	5 Hoe snei moet een meting in geval van de vijfjaarlijkse toet op de veiligheid uitgevoerd kunnen worden? U binnen 1 jaar na aanvraag U binnen 6 maanden na aanvraag U binnen 1 maanden na aanvraag U binnen 1 maand na aanvraag u anders, ni

Reacties op de vragenlijst ten behoeve van de ontwikkleing van een systeem voor de monitoring van zettingen en vervormingen van waterkeringen

	Dww-iR	HRS USHN	HRS Krimenpenerwaard	WS Vallei & EEM	HRS Alblasserwaard &
O naam	ir. A.A.M. Venmans		ing. D an Schie	P.G. Maiianhuic	Vimeerenlanden
Gatain diverigen	19 mei 1999	21 mei 1999	25 mer 1999	28 mei 1999	31 mei 1999
6 Hoe snel moelen de gegevens in geval van hoogwater					
Dinhen I week na uitvoeren van de vluchl					
Dinnen 3 dagen na ultvoeren van de vluchi	veringsbegeleiding		***************************************	***************************************	
binxen 1 dag na uitvoeren van de vluchi	, was a second		***************************************		
-	***************************************	, and a second	***************************************		
	***************************************	Č.	***************************************	X	
		zo snel mogelijk indien situalies bedreigend zijn	Υ		X
7 Hoe snei moeten de gegevens in geval van de vijfaartiikse					
toets op de velligheid beschikbaar komen?					
D binnen 3 maanden na uitvoeren van de vluchi					
	monitoring		***************************************		
binnen 2 weken na uilvoeren van de vlucht	Name of the last o		×	×	X
nnen 1 week na uitvoeren van de vlucht	***************************************	<u> </u>			
	***************************************		***************************************		***************************************
8 in welke opmaak moeten de gegevens aangeleverd					
worden? O in platte tekst oomaak (ASCIII)	>				
-	······································				
O in een tekenprogramma-opmaak nameliik	NOSC	-		Microsoft Excel	***************************************
D in een GIS-opmaak, namelijk	8	_	***************************************		AutoCad
anders, nl.	***************************************		Database organization		Aricinio, ArcCad
9 Zijn er nog onderwerpen, die niet in de voorgaande vragen aan de orde gekomen zijn, maar die wel aandacht behoeven? Zo ja, kunt u deze hier toelichten?		in siluates die bedreigend zijn, is het gelijktigg opnemen van een infra-tood (IfS) film Lb. het lokalsesten van kwelplekken newenst frechsisk F. Erkalan	Aprillada.	snelle inzetbaarheid en vtotte beschikbaarheid van resultaien is een voorwaarde voor de bruikbaarheid van het systeem	
				- van de zin van melingen lijdens hoogwater ben ik in het algemeen nog niet overluigd. De mensen in het veld levreen dan immers veel	

Appendix C - Beam steering

Before we are able to discuss the details of beam steering, the following angle definitions have to be clear:

- track: the angle between the north¹⁷ and the flight direction (= velocity vector direction) projected on the horizontal. Example: track= 180° if the aircraft flies to the south.
- heading: the angle between the north and the longer axis of the aircraft body projected on the horizontal. Example: if the nose points eastwards this angle is 90°.
- drift: track-heading (between -180° and 180°). Example: for the example above it equals 180-90= 90°.
- *pitch*: angle between the longer fuselage axis and the horizontal (between -180° and 180°) 18 . Positive if the nose of the aircraft points up.
- beam¹⁹ angle: the angle (between -180° and 180°) between an imaginary plane perpendicular to the longer antenna axis and the beam direction. Positive if the beam points forward.
- LOS: the angle between the north and the beam, measured in the horizontal plane.
- depression angle: the angle between the horizontal and the line connecting the target and the antenna.

During a flight *track*, *heading*, *drift*, *pitch* and *beam* are all available. Only the latter is fixed, until it changes (in 0.5 degree steps).

Fixed mode

To point the beam in the zero doppler direction (to prevent signal from falling outside the recorded frequency window) the beam is pointed perpendicularly to the velocity vector. This is done just before the datatake. During the datatake the beam is kept fixed.

The beam angle accomplishing this is computed as follows. Assume the beam angle and drift are 0. Due to a small pitch the angle between the beam and a line in the slant range plane (given by a depression angle θ) perpendicular to the velocity vector becomes $(pitch-3.5) \times \sin \theta$ (see footnote 18). Now assume the beam angle to be 0 and the pitch to be 3.5° (horizontal antenna condition). Due to a small amount of drift the same angle as before becomes $-drift \times \cos \theta$. The sum has to be compensated by the beam angle, so

$$beam = drift \times \cos\theta - (pitch - 3.5) \times \sin\theta. \tag{C.1}$$

^{17 &#}x27;North' refers in this appendix always to the geographical north. Furthermore, all angle are measured clockwise in the range 0 to 360°, unless indicated otherwise. For example: the angle between north and west 270°, not -90°.

¹⁸ The antenna is mounted at a downward angle of 3.5 with respect to the longer fuselage axis. Because the flying aircraft points upward by a few degrees on average, the antenna pitch, pitch-3.5°, is horizontal on average.

^{19 &#}x27;Beam' refers in this appendix to the main direction (i.e., the direction in which the power density is highest) of the beam.

Because beam depends on the depression angle θ , the zero doppler condition is never valid for the entire swath. Therefore a kind of mid-swath value is used for this parameter. This is also done for the other modes.

Active mode

The active mode differs from the drift mode only in that Eq.(C.1) is used every second during the datatake to update beam.

Geographic mode

In this mode the (projected) beam is pointed in a user provided LOS direction, fixed with respect to the north. This means that LOS is perpendicular to the desired track (i.e., a user supplied value), and drift is replaced by track-heading=LOS-270°-heading in Eq.(C.1), resulting in

$$beam = (LOS - 270^{\circ} - heading)\cos\theta - (pitch - 3.5) \times \sin\theta.$$
 (C.2)

As in the active mode, beam is updated every second during the datatake.

An example of the effect of this mode is illustrated in Figure C.1. For this figure the IRS-data from RPI-flight date June 1st 1999 were used to simulate the behaviour of the algorithm (i.e., to compute the LOS angle). For a LOS of 333° a track of 63° is desired. With the heading varying between 63.3° and 64.3° (IRS data), the LOS variation without beam steering would be 64.3-63.3= 1°. However, the beam steering limits the vatiation to about 333.3-332.7=0.6°. The plot shows the switching moments clearly. Note that the track is limited to the interval 62.8±0.1°, indicating a slight misalignment of the IRS. Guidance for the auto-pilot of the aircraft was obtained from a Position Reference System (PRS), which uses data from GPS, an additional GPS groundstation and data from the IRS. These data were fed through a Kalman filter, of which the output was compared to the desired track stored in the PRS. The output of the PRS was used to guide the auto-pilot.

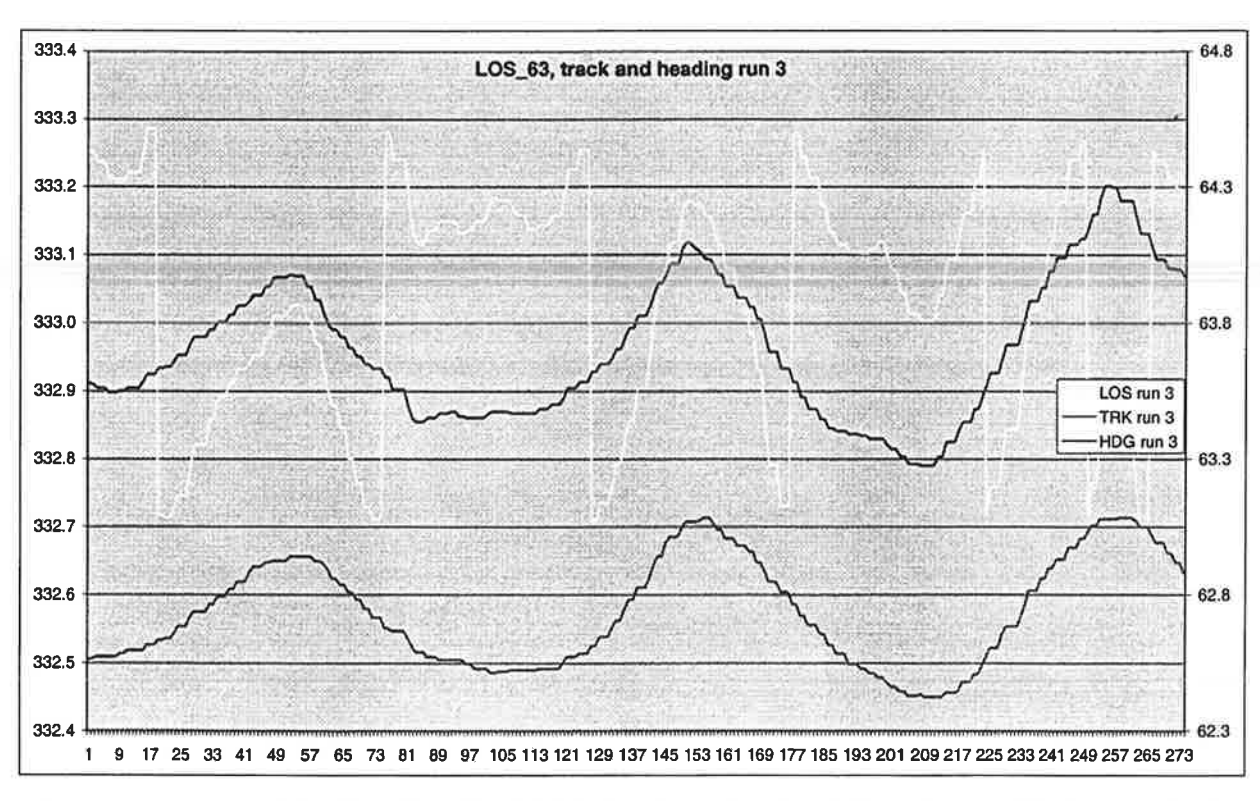


Figure C.1: LOS, track (TRK) and heading (HDG) plotted as a function of time (the unit of the horizontal axis is proportional to time). Note the different scales of the left (LOS) and right (TRK and HDG) axes.

The National Remote Sensing Programme 1990-2000, (NRSP-2) is implemented under the responsibility of the Netherlands Remote Sensing Board (BCRS) and coordinated by the Ministry of Transport and Public Works.

The objectives of the NRSP-2 are: to secure the long-term integration of the operationel use of remote sensing through temporary stimulation in the user-sectors of government and industry, to strengthen the development of remote sensing applications and the expansion of the national infrastructure.

Publication of:

Netherlands Remote Sensing Board (BCRS)
Programme Bureau,
Rijkswaterstaat Survey Department

P.O. Box 5023 2600 GA Delft The Netherlands

Tel.: +31 (15) 269 11 11 Fax: +31 (15) 261 89 62

E-mail: p.b.bcrs@mdi.rws.minvenw.nl

BCRS homepage: http://www.minvenw.ril/rws/mdi/bcrs